



## Research papers

# Borehole characterization of hydraulic properties and groundwater flow in a crystalline fractured aquifer of a headwater mountain watershed, Laramie Range, Wyoming

Shuangpo Ren<sup>a,b,\*</sup>, Samuel Gragg<sup>b</sup>, Ye Zhang<sup>b</sup>, Bradley J. Carr<sup>b</sup>, Guangqing Yao<sup>a</sup>

<sup>a</sup> Key Laboratory of Tectonics and Petroleum Resources of Ministry of Education, China University of Geosciences, Wuhan 430074, PR China

<sup>b</sup> Department of Geology and Geophysics, University of Wyoming, Laramie, WY, United States

## ARTICLE INFO

This manuscript was handled by P. Kitanidis, Editor-in-Chief, with the assistance of Simon A. Mathias, Associate Editor

## Keywords:

Fractured aquifer  
Slug test  
FLUTE profiling  
Borehole logging  
Hydraulic aperture  
Groundwater velocity and topographically driven flow

## ABSTRACT

Fractured crystalline aquifers of mountain watersheds may host a significant portion of the world's freshwater supply. To effectively utilize water resources in these environments, it is important to understand the hydraulic properties, groundwater storage, and flow processes in crystalline aquifers and field-derived insights are critically needed. Based on borehole hydraulic characterization and monitoring data, this study inferred hydraulic properties and groundwater flow of a crystalline fractured aquifer in Laramie Range, Wyoming. At three open holes completed in a fractured granite aquifer, both slug tests and FLUTE liner profiling were performed to obtain estimates of horizontal hydraulic conductivity ( $K_h$ ). Televiewer (i.e., optical and acoustic) and flowmeter logs were then jointly interpreted to identify the number of flowing fractures and fracture zones. Based on these data, hydraulic apertures were obtained for each borehole. Average groundwater velocity was then computed using  $K_h$ , aperture, and water level monitoring data. Finally, based on all available data, including cores, borehole logs, LIDAR topography, and a seismic P-wave velocity model, a three dimensional geological model of the site was built. In this fractured aquifer, (1) borehole  $K_h$  varies over ~4 orders of magnitude ( $10^{-8}$ – $10^{-5}$  m/s).  $K_h$  is consistently higher near the top of the bedrock that is interpreted as the weathering front. Using a cutoff  $K_h$  of  $10^{-10}$  m/s, the hydraulically significant zone extends to ~40–53 m depth. (2) FLUTE-estimated hydraulic apertures of fractures vary over 1 order of magnitude, and at each borehole, the average hydraulic aperture by FLUTE is very close to that obtained from slug tests. Thus, slug test can be used to provide a reliable estimate of the average fracture hydraulic aperture. (3) Estimated average effective fracture porosity is  $4.0 \times 10^{-4}$ , therefore this fractured aquifer can host significant quantity of water. (4) Natural groundwater velocity is estimated to range from 0.4 to 81.0 m/day, implying rapid pathways of fracture flow. (5) The average ambient water table position follows the boundary between saprolite and fractured bedrock. Groundwater flow at the site appears topography driven.

## 1. Introduction

A significant portion of the world's population relies on rivers that are sourced from fractured aquifers in mountain regions. In the western USA, alpine watersheds supply both surface water and groundwater to meet the water demands of over 60 million people (Barnett et al., 2005; Bales et al., 2006). In many parts of the world, especially in semi-arid to arid regions such as in India and Africa, groundwater in crystalline aquifers is the only source of drinking water (Gustafson and Krásný, 1994; Guihéneuf et al., 2014). To appropriately manage such resources, particularly in view of the projected warming in mountain environments compared to low lying regions (Pepin et al., 2015), new

hydrological knowledge about groundwater in mountain crystalline aquifers is required. However, groundwater storage and flow in most mountain environments are poorly known (Tague and Grant, 2009; Kurylyk and Hayashi, 2017). Mountain watersheds, which often consist of granitic or metamorphic rocks, are characterized with rough terrains that are difficult to access. Mountains are often sparsely populated, thus few groundwater monitoring wells exist from which long term water level or characterization data can be obtained. Surficial soil or vegetation covers in these environments are often thin or absent, giving rise to the perception that mountains are impervious to flow and thus have minimum storage for groundwater (Hood and Hayashi, 2015). However, groundwater flow and storage in alpine watersheds can constitute

\* Corresponding author at: Key Laboratory of Tectonics and Petroleum Resources of Ministry of Education, China University of Geosciences, Wuhan 430074, PR China.  
E-mail address: [cugspren@hotmail.com](mailto:cugspren@hotmail.com) (S. Ren).

a significant portion of the annual water budget, as demonstrated by Hood and Hayashi (2015). As water demands increase in the future, mountain environments, similar to the downstream regions, may become increasingly vulnerable to contamination.

This research aims to characterize a fractured crystalline aquifer in a headwater mountain watershed in Wyoming to understand both groundwater storage and groundwater flow. Results of this study will provide parameters for developing hydrological models to capture the properties and processes in the future. To quantify both groundwater storage and flow in a crystalline fractured aquifer, hydraulic aperture of fractures is a critical parameter to determine. On the one hand, the aperture provides information on fracture porosity and groundwater storage. On the other hand, the aperture can be used to calculate an average linear velocity that indicates the speed of groundwater flow through fractures. In order to obtain an estimate of the aperture, two parameters of the aquifer are often characterized: transmissivity or hydraulic conductivity of the aquifer, and the number of hydraulically active fractures.

Many hydraulic testing methods exist that can be used to obtain transmissivity or hydraulic conductivity of a fractured aquifer. Pumping tests, which are the most common method used in the field to interrogate large scale aquifer properties, can give an average horizontal hydraulic conductivity ( $K_h$ ) estimates over the entire producing zones of an aquifer (several tens of meters). Slug tests, by modeling water level response in a well due to rapid submergence and subsequently removal of a solid slug, can provide  $K_h$  estimate in the vicinity of the test well. Liquid slugs (i.e., addition/removal of fluid) can also be used to provide  $K_h$  estimates. Most commonly used analytical solutions for slug tests are (1) Hvorslev (1951) semi-log plot method for partial or fully penetrating wells in homogeneous confined or unconfined aquifers with negligible aquifer storativity, (2) Cooper et al. (1967) curve fitting method for fully penetrating wells in homogeneous confined aquifers, and (3) Bouwer and Rice (1976) method for completely or partially penetrating wells in homogeneous unconfined aquifers screened below the water table. All these methods are originally developed for homogeneous porous media. Shapiro and Hsieh (1998) compared the results of slug tests in fractured rock interpreted with a homogeneous (i.e., Cooper et al. (1967) solution) and a heterogeneous model. They found that the transmissivity estimated from both models are within one order of magnitude, thus equivalent transmissivity can be obtained from slug test results for strongly heterogeneous media. However, slug tests results can be skewed by non-ideal conditions in and adjacent to the wellbore. If a low permeability (positive) skin exists in a wellbore, both the Hvorslev (1951) and Bouwer and Rice (1976) methods are more likely to yield hydraulic conductivity estimates of the well-skin rather than that of the actual aquifer (Hyder et al., 1994; Hyder and Butler, 1995). As pointed out by Butler et al. (1996), the existence and nature of skin effects should be evaluated during the interpretation of slug tests.

Both the pumping and standard slug test (without packer system) methods, though commonly employed in the field, cannot resolve aquifer heterogeneity in the vertical direction. When vertical resolution of aquifer heterogeneity is required, high-resolution hydraulic testing methods are needed. For example, inflatable packers can be used to isolate one or more sections of a borehole for water injection or withdrawal during a well test (e.g., Cook, 2003; Quinn et al., 2012). Multilevel slug test is implemented by making use of a double-packer system to determine a series of  $K_h$  estimates for discrete depths in a well (e.g., Zlotnik and McGuire, 1998; Zlotnik and Zurbuchen, 2003; Zemansky and McElwee, 2005), while a dipole flow test is conducted by using a triple-packer system with a pump submerged in between two lower packers (e.g., Zlotnik et al., 2001). Other commonly used high-resolution borehole hydraulic methods include borehole flowmeter logging (e.g., Molz et al., 1989; Paillet, 1998; Paradis et al., 2011), direct push permeameter (e.g., Butler et al., 2007), and FLUTE liner profiling (e.g., Keller et al., 2014). All the hydraulic testing methods,

with the exception of the flowmeter logging, calls for the introduction or removal of a volume of water from the aquifer, which can pose issues at contaminated sites where contaminant mobilization and waste water disposal need to be minimized.

To determine the number of hydraulically active (i.e., flowing) fractures in a crystalline aquifer, borehole image logs and core logs can be used. However, large errors can arise in the interpretation of such logs. For example, micro-cracks are difficult to identify from borehole images, and core logs can contain drilling induced fractures that can be misidentified as formation fractures (Quinn et al., 2011a,b). Moreover, not all fractures identified are necessarily hydraulically active. For a fractured dolostone aquifer, Quinn et al. (2011a,b) proposed a method for identifying flowing fractures that naturally exist in the formations. They used constant-head step tests with increasing injection rates to determine a set of critical flow rates and critical Reynolds ( $Re_c$ ) numbers when non-Darcian flow started to develop. Their method employs an iterative procedure by changing the assumed number of flowing fractures in each test interval until a high correlation coefficient between  $Re_c$  and calculated aperture was reached. However, their method was effective only under high flow rates that induce non-Darcian flow, while for Darcian flow regimes, the method is not applicable.

For a crystalline fractured aquifer in a headwater mountain watershed in Wyoming, this study aims to estimate both  $K_h$  and the number of hydraulically active fractures in order to obtain fracture aperture data. We conducted a detailed aquifer characterization study using borehole televiwer logs, flowmeter logs, and borehole hydraulic tests (specifically, slug tests and FLUTE blank liner profiling) on three boreholes that tap into this aquifer. Our research took place at the Blair Wallis Fractured Rock Hydrology Research Well Field, which lies in the Laramie Range in southeastern Wyoming, where nine bedrock wells have been drilled and completed at various depths. The three boreholes investigated cover a range of depth and fracture intensity at the site, and were thus selected for a focused hydraulic characterization study. By jointly interpreting results from all borehole tests, both transmissibility ( $T$ ) and horizontal hydraulic conductivity ( $K_h$ ) were obtained at different vertical resolutions. The number of flowing fractures for the same tested intervals were determined by jointly interpreting borehole televiwer (i.e., optical and acoustic) and impeller flowmeter logging under ambient flow conditions. Finally, hydraulic apertures at various vertical scales were determined, based on which fracture porosity and groundwater velocity under ambient flow condition were also estimated. The implications of our results at the well field are discussed at the watershed scale to infer the importance of bedrock groundwater in the mountain environment.

## 2. Study site

Most crystalline aquifers consist of three zones: an upper weathered zone, a middle fractured zone, and a lower and often less fractured zone (Krásný and Sharp, 2003). The Blair Wallis Fractured Granite Hydrology Research Well Field lies within the Crow Creek Watershed of the Laramie Range which lies within US Forest Service land about 21 km southeast of Laramie, Wyoming (Fig. 1(a) and (b)). Local climate data from the Crow Creek SNOTEL station of the last 10 years show that the Blair Wallis well field has a mean annual temperature of 5.4 °C and receives 620 mm of annual precipitation, of which 90% falls as snow (National Resources Conservation Service, 2015). During the summer season (June to September), average temperature is around 15 °C, while in the winter months (December to March), average temperature is around -5 °C. The geology of the well field consists of fractured granite bedrock overlain by 10–18 m of weathered granite (saprolite). Based on jointly interpretation of both borehole televiwer logs and flowmeter logs at the site, bedrock flowing fracture intensity diminishes with depth. Based on water level monitoring data collected from the well field, the fractured bedrock is saturated with groundwater while the saprolite is either unsaturated or partially saturated. By examining

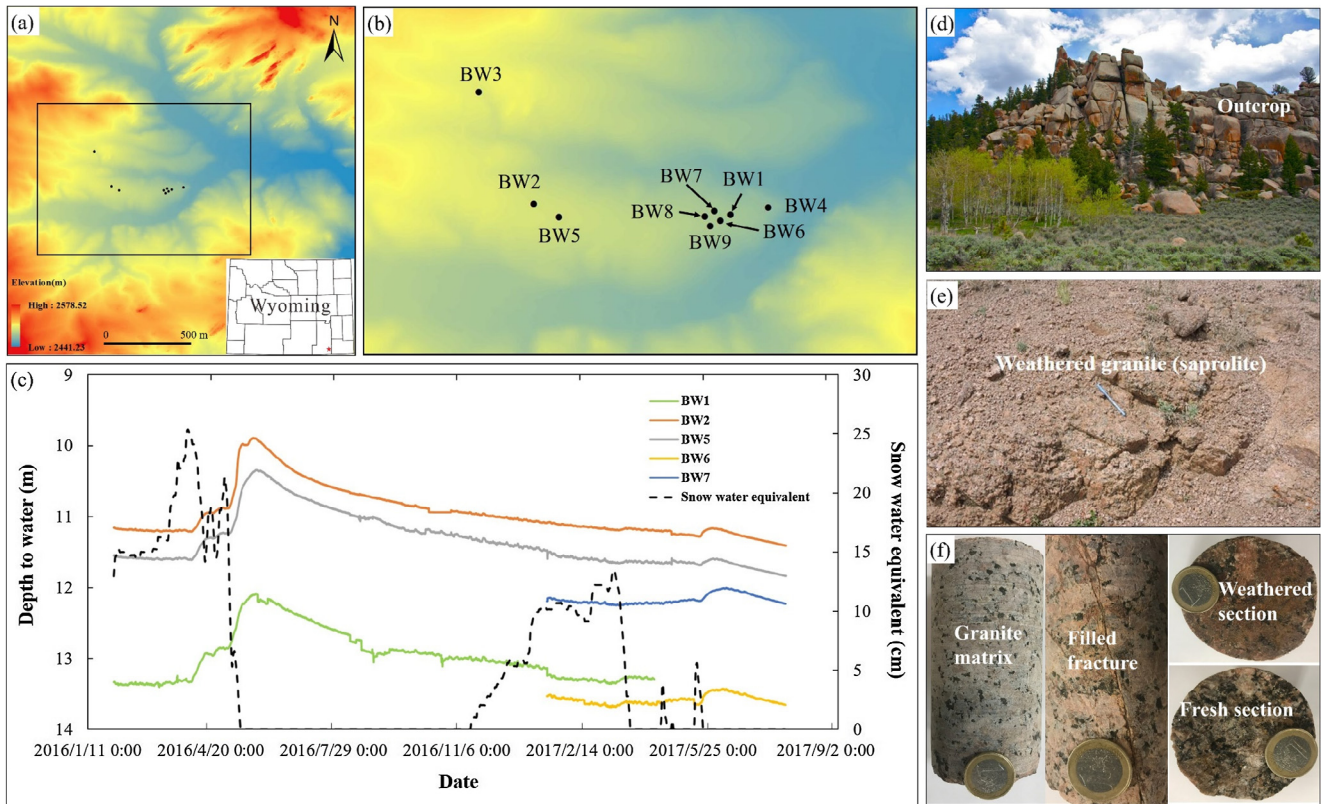


**Fig. 1.** (a)–(b) Map of the Blair Wallis Fractured Rock research well field, (c) Plot of monitored depth to water from BW 1, 2, 5, 6, and 7, and snow water equivalent (data are from the Crow Creek SNOTEL), (d) an outcrop at the field site, (e) a photo of saprolite of ground surface, and (f) bedrock core samples from BW5. Depth to water is measured from top of casing.

groundwater level data against snow water equivalent data from a SNOTEL station that lies northeast ~6 km from the well field, groundwater in the fractured bedrock aquifer is recharged primarily from snowmelt infiltration in the Laramie Range which occurs in late spring (Fig. 1(c)). Note that only water level data from BW 1, 2, 5, 6, and 7 are shown, which captures the range of water level variability in the well field.

At the Blair Wallis well field, nine bedrock wells have been completed that are cased to the bottom of the saprolite but remain open boreholes in the fractured granite. A well schematic is shown in Fig. 2. This research focuses hydraulic characterization of three of these bedrock wells (i.e., BW5, BW6, and BW7) which lie within the so called A-type Sherman Granite which are generated 1.43 Ga ago consisting of microcline, plagioclase, quartz, hornblende, biotite, and ilmenite (Frost et al., 1999). The configuration of these three wells are summarized in Table 1. Based on the completion data of each well and the monitored water level responses, these three wells lie in an unconfined aquifer. Furthermore, from FLUTE liner profiling of the three wells (presented later), borehole transmissivity becomes negligible below approximately 40–53 m bgs, which corresponds to observed lower frequency of flowing fractures beneath this depth. Thus, each borehole is considered fully penetrating in the slug test interpretation.

### 3. Methods

#### 3.1. Slug test

A standard slug test involves a rapid submergence and subsequently removal of a solid slug from a well casing or a borehole. The water level responses were recorded and modeled by fitting them to the solution of a radial groundwater flow equation to obtain a horizontal hydraulic conductivity estimate. For confined and unconfined aquifers, both

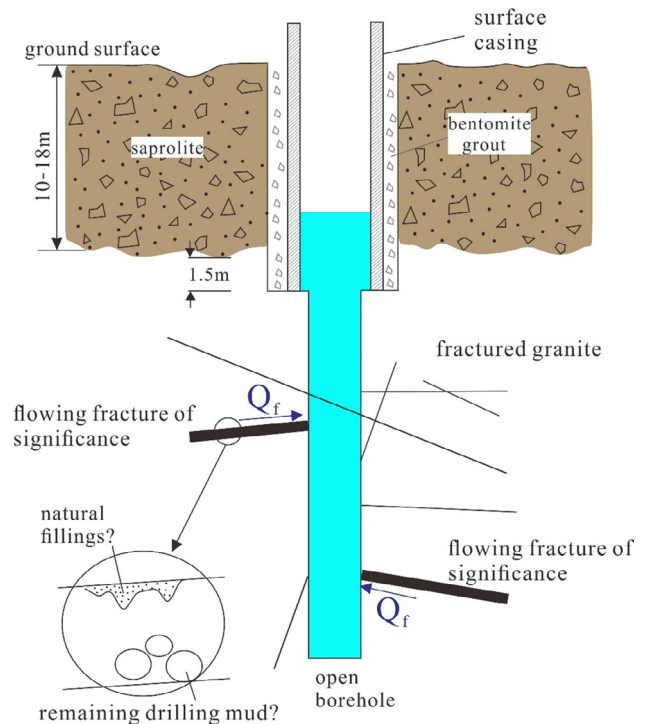


**Fig. 2.** Schematics of Blair Wallis bedrock well.

steady state and transient slug test solutions exist. For example, besides  $K_b$  storativity of the aquifer can be additionally determined using the transient solution. Besides water level responses, however, other factors can lead to inaccurate parameter estimates, e.g., well-skin and non-

**Table 1**  
Configuration of the three bedrock wells investigated in this study.

	BW5	BW6	BW7
Total depth (m - bgs)	39.02	60.76	72.83
Casing depth (m - bgs)	18	17.07	17.07
Open hole length (m)	21.02	43.69	55.76
Casing diameter (inch)	4" PVC casing	6" PVC casing	6" PVC casing
Open hole diameter (inch)	~3.8"	5"	5"
Rock type	A-type Granite	A-type Granite	A-type Granite
DTW on slug test date (m) <sup>1</sup>	11.45	13.59	12.18
Drilling method	Drilled with water; airlift development	Air/water rotary + downhole hammer; airlift development	Air/water rotary + downhole hammer; airlifted development
Initial displacement for different slug size (m)	0.59/0.33	0.54/0.23	0.63/0.25

<sup>1</sup> DTW are measured from top of casing: the value reported here were measured before the initiation of the slug tests.

Darcian flow can lead to a significantly underestimated  $K_h$  (e.g., Quinn et al., 2013). For different aquifers and well completions, Butler et al. (1996) reported a series of guidelines to improve the quality of parameter estimates obtained from slug tests. These guidelines were followed in the slug tests we carried out at the Blair Wallis well field in order to obtain representative near-wellbore  $K_h$  estimates and ensure that non-ideal behaviors can be identified and properly interpreted. This article reports the results of slug tests at BW5, BW6, BW7, which were carried out in late May and early June of 2017.

For a given slug test, given the diameter of the open borehole, two sizes of solid slugs were used to generate two different initial water level displacement ( $H_0$ ) at each well. For BW5, the larger slug is 162.6 cm long and 6 cm diameter, and the small slug is 120 cm long and 5 cm diameter. For BW6 and BW7, the same set of slugs were used with dimensions of: 184.2 cm long and 9.4 cm diameter (large), and 162.6 cm long and 6 cm diameter (small). At BW5 and BW7, the sequence of slugs used was "large-small-large" to evaluate borehole effects such as dynamic skin (Butler, 1998): (1) the large slug was first used to perform a set of slug-in (falling head, or FH) and slug-out (rising head, or RH) tests. The same set of slug-in and slug-out tests were repeated. (2) the small slug was used to perform a new set of slug-in and slug-out tests, which were also repeated. (3) step (1) is repeated using the large slug. At BW6, due to the extremely slow water level recovery rate, step (3) was carried out using the large slug only once. Thus, six rising head tests and six falling head tests were performed at BW5 and BW7, and five rising head tests and five falling head tests were performed at BW6. For each well, two different  $H_0$  were generated with a maximum  $H_0$  around 0.6 m (Table 1). Given the moderate level of  $H_0$ , during both FH and RH tests for each well, water level was always within the casing, thus the borehole was not de-saturated during the RH test.

The water level data from the slug tests were analyzed using the Bouwer-Rice method for a fully penetrating well in an unconfined aquifer (Bouwer and Rice, 1976):

$$K_h = \frac{r_c^2 \ln(r_e/r_w)}{2L} \frac{1}{t} \ln \frac{H_0}{H_t} \quad (1)$$

where  $K_h$  is near-wellbore average horizontal hydraulic conductivity of the open hole interval,  $r_c$  is casing radius,  $L$  is the length of open hole,  $r_e$  is an influence radius in the formation at which there is assumed to be no change in hydraulic head,  $r_w$  is the radius of the open hole,  $t$  is elapsed time from start of a slug test,  $H_0$  is initial displacement at  $t = 0$ , and  $H_t$  is the displacement at time  $t$ . The transmissivity of each open hole can then be determined by:  $T = K_h L$ . Moreover, at the Blair Wallis well field, the magnitude of hydraulic gradient of 0.04 was averaged from September 2015–September 2016. During the dry winter season (September–March), the magnitude was between 0.03 and 0.04; during the snowmelt season in spring, the magnitude was between 0.04 and 0.05; in May and June, the magnitude sometimes reached 0.05. Thus, for year 2015–2016, the magnitude of the head gradient was quite

stable, ranging from ~0.03 to ~0.05. In this study, an average horizontal hydraulic gradient of 0.04 will be used to calculate the groundwater velocity. According to the long term water level data, we can assume that the gradient direction is roughly from east to west and thus groundwater flow direction is roughly west to east if horizontal isotropy can be assumed. Moreover, based on our analysis of water level trends over time, direction of the overall head gradient vector does not change significantly over time. Classic slug test solutions developed for a confined aquifer (i.e., Cooper et al., 1967) was also applied to interpreting the same slug tests done in this unconfined aquifer. This solution is also a transient flow solution which can lead to the estimation of the specific storage coefficient ( $S_s$ ) which reflects the elastic storage of the aquifer.

During a slug test, if the induced groundwater velocity is high, non-Darcian flow can occur whereas head gradient is not linearly related to the flow rate into and out of the formation. Hydraulic head responses under non-Darcian flow, when interpreted using the standard slug test solutions derived for laminar flow, can lead to underestimated  $K_h$  and consequently underestimated hydraulic aperture  $b$  (e.g., Quinn et al., 2011a,b). To test for non-Darcian flow in granular deposits, Butler et al. (1996) pointed out the need to carry out a series of slug tests with different  $H_0$ . Non-Darcian flow can be identified by fitting to the classic solutions, such as Hvorslev semi-log plots and Cooper curve fitting. For both porous and fractured rocks, a strong dependence of the estimated  $K_h$  on  $H_0$  is considered evidence of non-Darcian flow (Butler et al., 1996; Quinn et al., 2013; Ji and Koh, 2015). Such dependence is exhibited as an increasingly lower value of estimated  $K_h$  with increasing slug size.

To determine if non-Darcian flow has occurred during slug tests in a formation with a single fracture, a Reynold number ( $Re$ ) can be defined (Ji et al., 2008; Ji and Koh, 2015):

$$Re = \frac{\rho_w v b}{\mu} = \frac{\rho Q}{w \mu} \quad (2)$$

where  $\rho_w$  [M/L<sup>3</sup>] is density of groundwater,  $v$  [L/T] is flow velocity in the fracture,  $b$  [L] is fracture aperture,  $\mu$  [M/LT] is fluid viscosity,  $Q$  [L<sup>3</sup>/T] is flow rate in the fracture, and  $w$  [L] is the fracture width perpendicular to flow. Laboratory experiments with single-fracture models indicate that non-Darcian flow can be significant when  $Re$  is greater than 1–10 (e.g., Zimmerman et al., 2004; Ranjith and Darlington, 2007; Ji et al., 2008).

Given that hydraulic conductivity of granite matrix is on the order of 10<sup>-13</sup> m/s (e.g., Mohnke and Yaramanci, 2008), we assume that during the slug tests, groundwater flowed into/out of the wellbore only through flowing fractures. Therefore, a mean flow rate can be calculated as:

$$Q_{mean} = \frac{\sum_{i=1}^N Q_i}{N} \quad (3)$$

where  $Q_i$  [ $L^3/T$ ] is the flow rate at the  $i$ -th fracture and  $N$  is the number of flowing fractures in the tested zone. Because during both RH and FH tests at BW 5, 6, and 7, the water level in the borehole is always within the casing, the total flow rate can be given as:

$$\sum_{i=1}^N Q_i = \frac{\pi r_c^2 \Delta h}{\Delta t} \quad (4)$$

where  $r_c$  [L] is radius of the casing and  $\Delta h$  [L] is change of hydraulic head in the tested interval during time  $\Delta t$  [T]. In this study, for each flowing fracture, water level change in the borehole per second was used to calculate an average  $Re$ . Note that the  $Re$  computed using Eqs. (2–4) is a mean value over all the flowing fractures in a borehole and it is likely that  $Re$  of individual fractures vary from the mean. For a granitic aquifer with several fractures, Ji and Koh (2015) found that non-Darcian flow can be generated when an average  $Re$  reached  $\sim 3$ . This suggests that for media with multiple fractures, non-Darcian flow is possible when  $Re$  is relatively small.

### 3.2. Flute liner profiling

FLUTE profiling is a high-resolution hydraulic testing method for estimating  $T$  or  $K_h$  along an open borehole (see Keller et al., 2014 for details). Compared to the standard packers tests, FLUTE profiling can yield  $T$  estimates cost effectively and is considered suitable for delineating flow zones in strongly heterogeneous porous and fractured rocks. A suite of FLUTE blank liner and one-time hydraulic head profiling were performed below the casings of BW5, BW6 and BW7 to identify permeable fractures along the open holes, their transmissivity profiles, as well as the formation head distribution at the time of the profiling.

At the beginning of the liner profiling method, a flexible fabric cylinder (open at the top and closed at the bottom) was installed at the top of casing. Water was filled into the liner to create a hydraulic head differential between the inside and outside of the liner which pulls the liner downward. While the liner travels down the borehole, it pushes water beneath the liner from the open hole into the formation through transmissive fractures. At each depth, the descent rate of the liner is positively correlated with the transmissivity of the remaining length of the open hole beneath the liner. As the liner goes down, its descent rate decreases because the transmissive features of the open hole are gradually sealed off. The liner velocity was measured using two encoders that are placed on a meter roller which recorded the position of the liner over every 0.5 s during profiling. This technique also allows the measurement of a large velocity range or liner descent rate (Keller et al., 2014). A volumetric flow rate can be determined from the descent rate, while head gradients can be calculated from transducers placed above and beneath the liner. A transmissivity can then be estimated using the Thiem equation assuming steady state radial flow from borehole into the formation:

$$T = \frac{\Delta Q}{2\pi \Delta H} \ln\left(\frac{r_e}{r_w}\right) \quad (5)$$

where  $\Delta Q$  [ $L^3T$ ] is the flow rate,  $T$  [ $L^2/T$ ] is the transmissivity of a measured interval,  $\Delta H$  [L] is the applied head difference,  $r_e$  [L] is an influence radius in the formation at which there is assumed to be no change in hydraulic head, and  $r_w$  [L] is the radius of the open hole.

However, detection limit of FLUTE liner profiling is a function of the descent velocity, and small velocity changes can be difficult to detect if the descent velocity is high. Thus,  $T$  estimates obtained from FLUTE profiling may be less accurate and precise than the short interval straddle packer tests (Quinn et al., 2015). However, compared to packer tests, FLUTE profiling is less time consuming and can often circumvent the leakage issues due to the existence of preferential flow paths between packers (Keller et al., 2014). Such preferential flow paths often characterize strong heterogeneous media such as the fractured granite

that we investigate in this work.

### 3.3. Borehole televiewer and flowmeter logging

At each well, QL40-ABI-2G Borehole Televiewer (i.e., optical and acoustic) and QL40-SFM Spinner Flowmeter (Mt. Sopris Instrument, Denver, CO) logging were jointly interpreted to identify flowing fractures along the open hole. Borehole televiewer logs, either optical and acoustic, can be used to identify apparent fractures along the borehole wall, but micro-cracks cannot always be identified from borehole televiewer. Also, the identified fractures from such logs are not always hydraulically active.

Under ambient flow, flowmeter logging can be used to detect variation of vertical flow rates along an open hole, and significant flow rate differences between adjacent positions can indicate the approximate location of a flowing fracture or fractured zone. Additionally, flowmeter logging can be used to detect flowing micro-cracks which provide conduits for groundwater but cannot be identified by the borehole televiewer. At BW5, 6, and 7, impeller flowmeter logs were obtained which yield a flow rate profile that can be used to filter out flowing fractures from fractures identified from borehole televiewer logs, also the “equivalent” flowing micro-cracks which cannot be seen from borehole televiewer logs. By a combined interpretation of borehole televiewer and flowmeter logging, the number of equivalent flowing fractures can be obtained for a given borehole.

Here we emphasize that cores were only used as reference for identifying flowing fractures. This is because (1) at the Blair Wallis field site, only five of nine bedrock wells were cored (i.e., BW1, BW2, BW3, BW4 and BW5) and BW6, BW7, BW8 and BW9 were not cored; (2) there are a number of drilling-induced fractures in the cores which do not represent the actual borehole condition. For BW5 where we have both core and logging data, we can examine fractures jointly (Fig. 3). Some of the observed fractures in cores with weathered surfaces suggest that they are natural fractures. These are also identified by examining the logging data at the same depth interval, which suggests the reliability of the logging data. There are also a few drilling induced fractures in cores: these do not exist along the wellbore and can therefore not be identified from the borehole logging data. For BW6 and BW7, we only have logging data with which flowing fractures were identified.

### 3.4. Hydraulic aperture determination

By solving the one-dimensional Navier–Stokes equations for laminar flow in a single, parallel, smooth-walled planar fracture, Romm (1966) obtains the Cubic Law:

$$Q_x = \frac{\rho_w g b^3 w}{12\mu} \frac{\partial h}{\partial x} \quad (6)$$

where  $\rho_w$  is the water density [ $M/L^3$ ],  $g$  is gravity acceleration [ $L/T^2$ ],  $b$  is the hydraulic aperture of the fracture [L],  $w$  is the width of the fracture normal to flow [L],  $\mu$  is the dynamic viscosity of water [ $M/LT$ ], and  $\partial h/\partial x$  is the hydraulic gradient in the direction of flow [–]. For a set of parallel uniform fractures, Snow (1965) further derived an equation relating the equivalent transmissivity and an average hydraulic aperture:

$$T = \frac{\rho_w g N b^3}{12\mu} \quad (7)$$

where  $N$  is the number of hydraulically active fractures in the test interval [–]. However, Eq. (7) assumes that all fractures are identical. If it is applied to non-uniformly distributed fractures with variable apertures, the single estimated  $b$  thus reflects an average hydraulic aperture (Quinn et al., 2011a,b). Based on Eq. (1), substituting the calculated  $T$  values and the number of flowing fractures  $N$  into Eq. (7), an average hydraulic aperture can be written as:

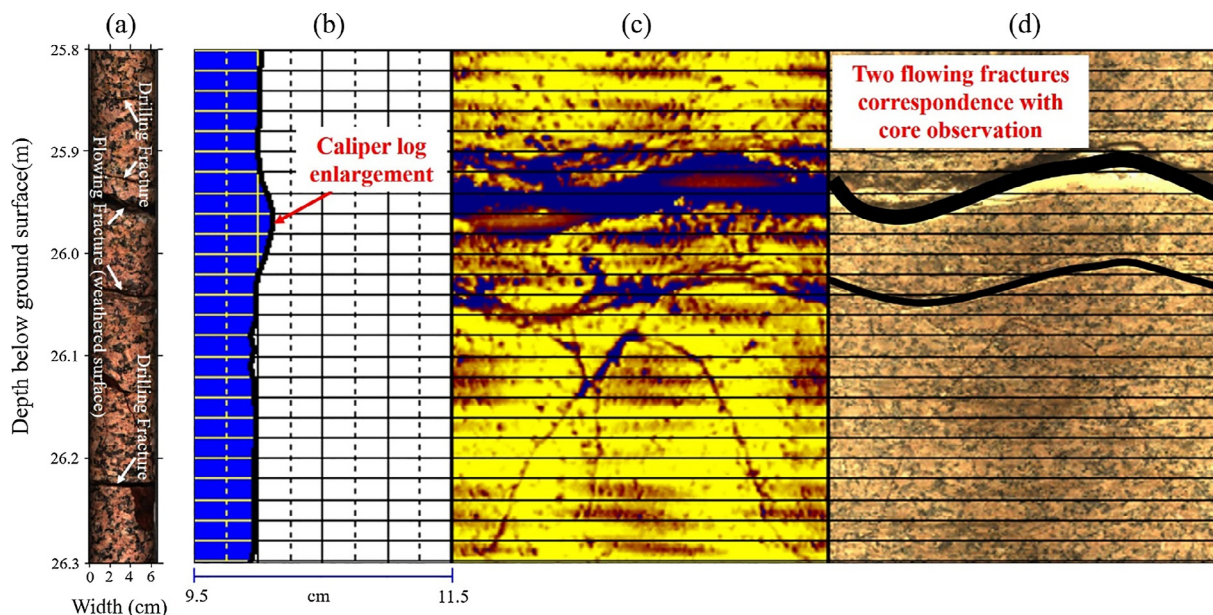


Fig. 3. Fractures observed in cores (a) and their correspondence with (b) Caliper, (c) ABI, and (d) OBI logs at BW5 at the same depth interval.

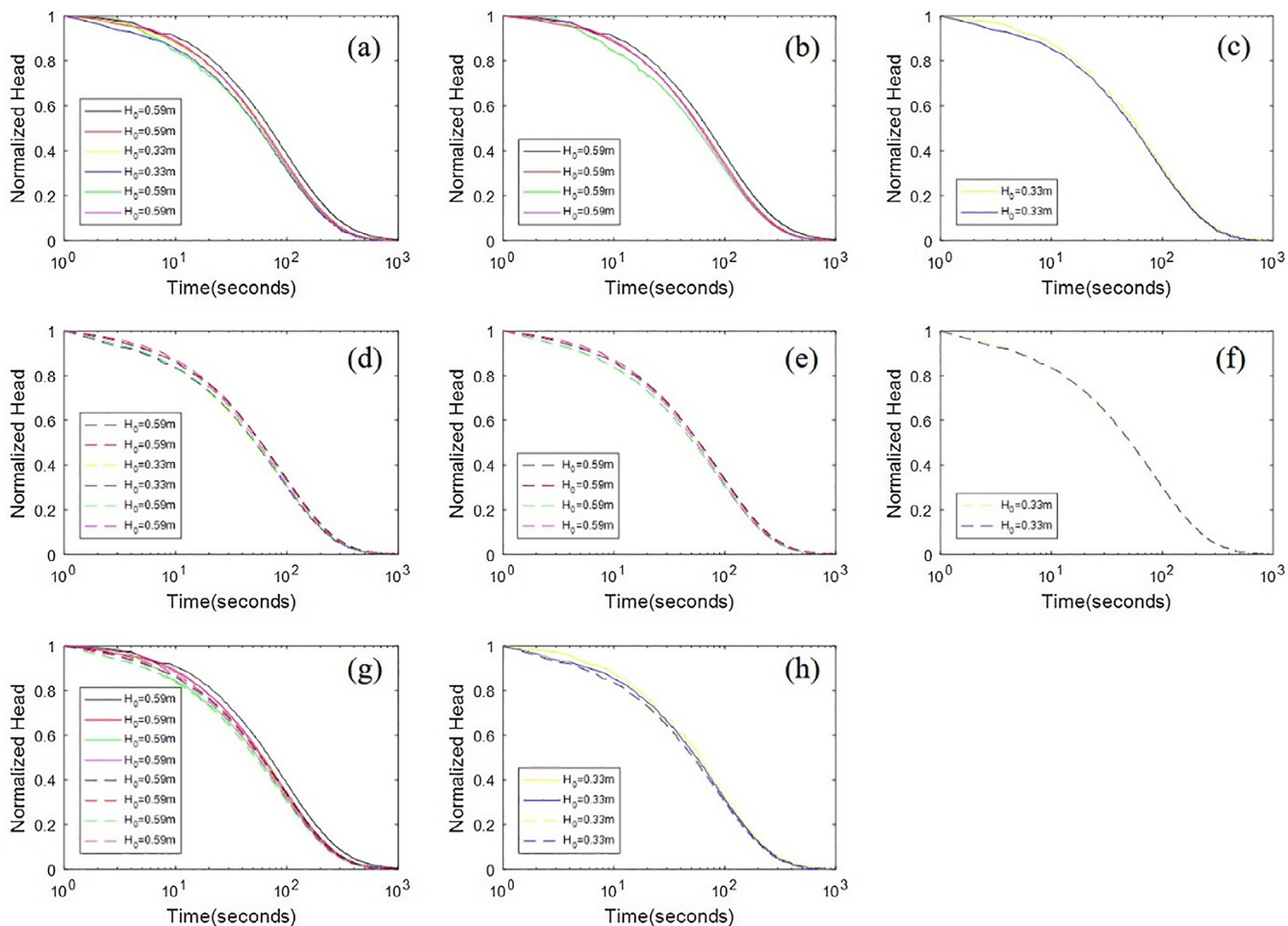


Fig. 4. Normalized head ( $H(t)/H_0$ ) vs. log time for series of RH and FH slug tests performed in well BW5. (a) All FH tests performed in BW5. (b) FH test with the large  $H_0$ . (c) FH test with the small  $H_0$ . (d) All RH tests performed in BW5. (e) RH tests with the large  $H_0$ . (f) RH tests with the small  $H_0$ . (g) RH and FH test with the large  $H_0$ . (h) RH and FH slug test with the small  $H_0$ . Solid lines indicate FH tests and dashed lines indicate RH test.

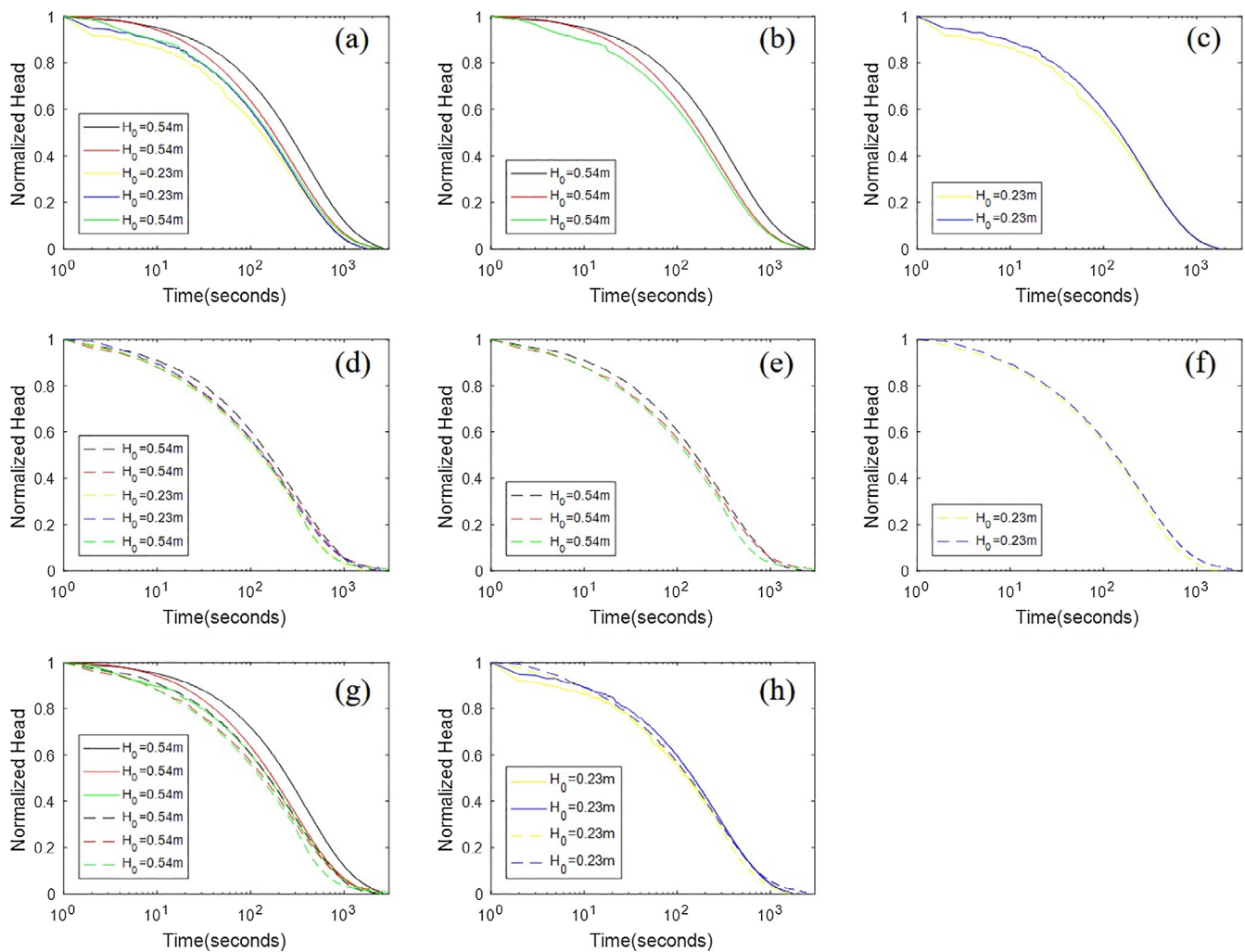


Fig. 5. Normalized head ( $H(t)/H_0$ ) vs. log time for series of RH and FH slug tests performed in well BW6. (a) All FH tests performed in BW6. (b) FH test with the large  $H_0$ . (c) FH test with the small  $H_0$ . (d) All RH tests performed in BW6. (e) RH tests with the large  $H_0$ . (f) RH tests with the small  $H_0$ . (g) RH and FH test with the large  $H_0$ . (h) RH and FH slug test with the small  $H_0$ . Solid lines indicate FH tests and dashed lines indicate RH test.

$$b = \sqrt[3]{\frac{12\mu T}{\rho_w g N}} \quad (8)$$

In this research, different hydraulic tests can lead to an estimated  $K_h$  or  $T$  for different support volumes, thus the aperture calculated using Eq. (8) can yield  $b$  at various resolutions.

## 4. Results and discussion

### 4.1. Slug test results and analysis

#### 4.1.1. Qualitative analysis of well-skin effect

Theories have pointed out that, when there is no well-skin effect, the duration of a slug test would be independent of the normalized head, i.e.,  $H(t)/H_0$  (e.g., Butler et al., 1996). This suggests that when the normalized head is plotted against time for a series of slug tests with different  $H_0$ , the curves of the normalized head would coincide. Figs. 4–6 plot the slug test results for BW5, BW6, and BW7, respectively, under two different  $H_0$ . As shown in Fig. 4 and Fig. 6, because all the curves almost completely coincide (especially during the rising head tests), skin effect for BW5 and BW7 is considered negligible. In BW6 (Fig. 5), however, the normalized water level responses do not coincide exactly, especially when the  $H_0$  is relatively large, may suggest a skin effect. Both airlift and step tests carried out in BW6 in October 2016 have produced sediments consisting of clay and granite minerals. The

sediment production suggests that fractures near the borehole contain infills that can be mobilized during the slug test. In comparison, no or very limited sediments were produced during the same airlift tests of BW5 and BW7.

For the three wells, a set of horizontal hydraulic conductivity were estimated using both the Cooper et al. (1967) curve fitting solution and the Bouwer–Rice model (Bouwer and Rice, 1976). Results are summarized in Table 2, which presents the set of  $K_h$  estimated for each well under both FH and RH conditions and for the repeat tests as well. Based on these  $K_h$  estimates, a mean and a standard deviation were obtained for each well. The standard deviations generally are on the order of  $10^{-7}$  or smaller, suggesting that the estimated  $K_h$  are reliable with low uncertainty. Furthermore, for each well, the ratio between the highest estimated  $K_h$  and the lowest estimated  $K_h$  is less than 1.5, which suggests that any skin effect exhibited during the slug test (i.e., BW6) is hydraulically insignificant and may not need to be accounted for in the slug test interpretation using the classic solutions.

For BW5 and BW7,  $K_h$  estimates using the Cooper et al. (1967) solution are more than twice as large as those estimated using the Bouwer–Rice model. To explain this deviation, Butler et al. (1996) pointed out that the Cooper et al. model can lead to a significantly over-estimated  $K_h$  of the formation when a dimensionless storage parameter ( $\alpha$ ) of the formation is moderate to low:

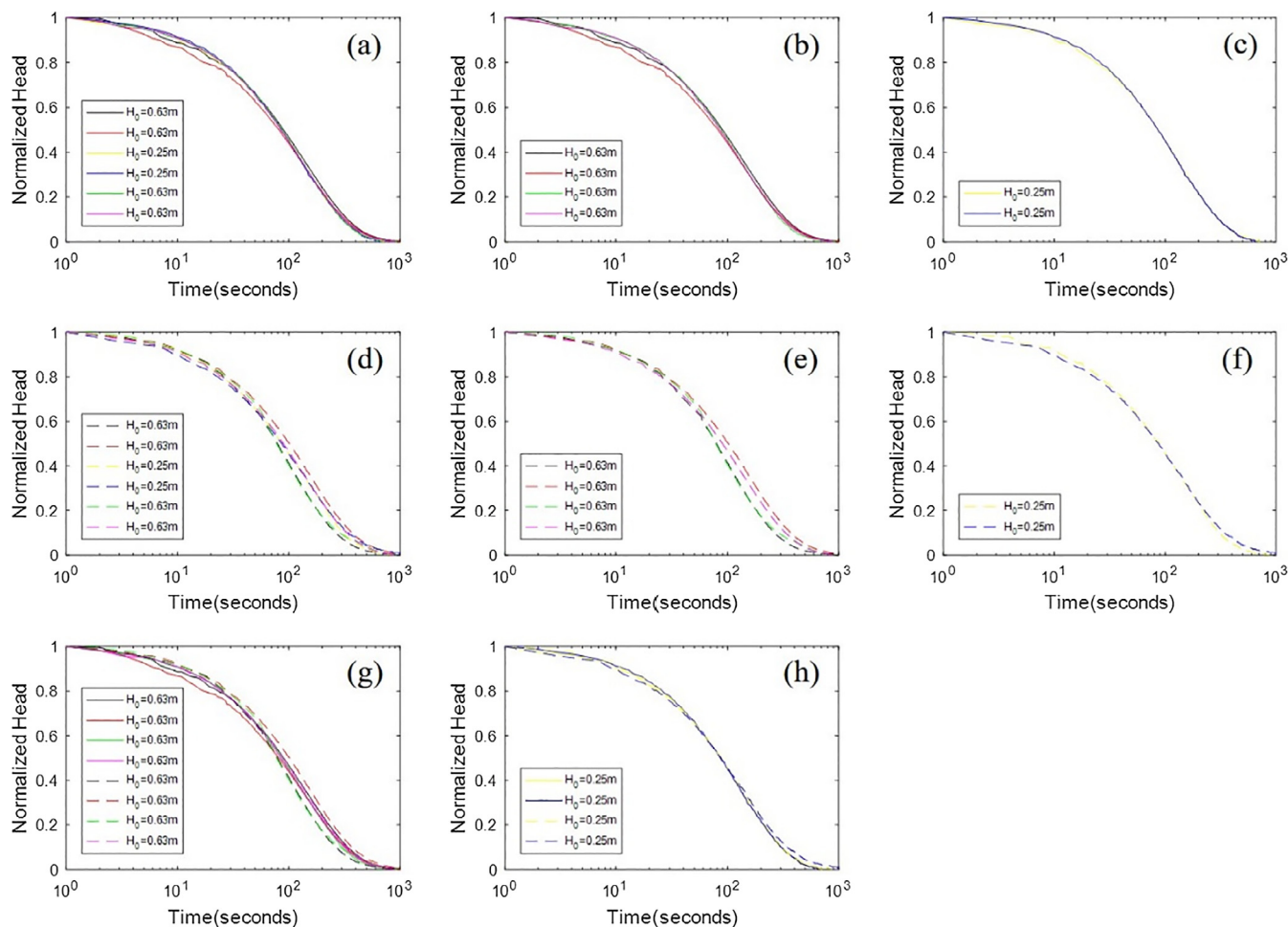


Fig. 6. Normalized head ( $H(t)/H_0$ ) vs. log time for series of RH and FH slug tests performed in well BW7. (a) All FH tests performed in BW7. (b) FH test with the large  $H_0$ . (c) FH test with the small  $H_0$ . (d) All RH tests performed in BW7. (e) RH tests with the large  $H_0$ . (f) RH tests with the small  $H_0$ . (g) RH and FH test with the large  $H_0$ . (h) RH and FH slug test with the small  $H_0$ . Solid lines indicate FH tests and dashed lines indicate RH test.

Table 2

$K_h$  estimated (in m/s) based on Cooper et al. (1967) and Bouwer–Rice (1976) model.

Well	Sequence number	Cooper et al. (1967) model		Bouwer–Rice (1976) model	
		FH	RH	FH	RH
BW5	Big $H_0$	$7.10 \times 10^{-6}$	$6.60 \times 10^{-6}$	$3.02 \times 10^{-6}$	$3.11 \times 10^{-6}$
	Big $H_0$	$8.40 \times 10^{-6}$	$6.60 \times 10^{-6}$	$3.08 \times 10^{-6}$	$3.06 \times 10^{-6}$
	Small $H_0$	$8.90 \times 10^{-6}$	$7.70 \times 10^{-6}$	$3.09 \times 10^{-6}$	$3.09 \times 10^{-6}$
	Small $H_0$	$9.10 \times 10^{-6}$	$5.60 \times 10^{-6}$	$3.07 \times 10^{-6}$	$3.13 \times 10^{-6}$
	Big $H_0$	$6.90 \times 10^{-6}$	$5.40 \times 10^{-6}$	$3.08 \times 10^{-6}$	$3.08 \times 10^{-6}$
	Big $H_0$	$8.40 \times 10^{-6}$	$5.00 \times 10^{-6}$	$3.13 \times 10^{-6}$	$3.06 \times 10^{-6}$
Arithmetic mean		$8.13 \times 10^{-6}$	$6.15 \times 10^{-6}$	$3.08 \times 10^{-6}$	$3.09 \times 10^{-6}$
Standard deviation		$9.22 \times 10^{-7}$	$9.99 \times 10^{-7}$	$3.31 \times 10^{-8}$	$2.93 \times 10^{-8}$
BW6	Big $H_0$	$7.30 \times 10^{-7}$	$7.50 \times 10^{-7}$	$7.54E \times 10^{-7}$	$9.50 \times 10^{-7}$
	Big $H_0$	$1.00 \times 10^{-6}$	$8.80 \times 10^{-7}$	$9.56E \times 10^{-7}$	$1.02 \times 10^{-6}$
	Small $H_0$	$8.50 \times 10^{-7}$	$9.50 \times 10^{-7}$	$9.82E \times 10^{-7}$	$1.12 \times 10^{-6}$
	Small $H_0$	$8.50 \times 10^{-7}$	$9.00 \times 10^{-7}$	$1.05 \times 10^{-6}$	$9.67 \times 10^{-7}$
	Big $H_0$	$7.90 \times 10^{-7}$	$9.40 \times 10^{-7}$	$1.03 \times 10^{-6}$	$9.72 \times 10^{-7}$
	Big $H_0$	$8.44 \times 10^{-7}$	$8.84 \times 10^{-7}$	$9.55 \times 10^{-7}$	$1.01 \times 10^{-6}$
Arithmetic mean		$8.44 \times 10^{-7}$	$8.84 \times 10^{-7}$	$9.55 \times 10^{-7}$	$1.01 \times 10^{-6}$
Standard deviation		$8.98 \times 10^{-8}$	$7.17 \times 10^{-8}$	$1.06 \times 10^{-7}$	$6.16 \times 10^{-8}$
BW7	Big $H_0$	$3.70 \times 10^{-6}$	$5.60 \times 10^{-6}$	$1.99 \times 10^{-6}$	$2.64 \times 10^{-6}$
	Big $H_0$	$3.90 \times 10^{-6}$	$4.50 \times 10^{-6}$	$1.96 \times 10^{-6}$	$1.81 \times 10^{-6}$
	Small $H_0$	$3.90 \times 10^{-6}$	$5.20 \times 10^{-6}$	$2.19 \times 10^{-6}$	$2.17 \times 10^{-6}$
	Small $H_0$	$3.80 \times 10^{-6}$	$3.80 \times 10^{-6}$	$2.21 \times 10^{-6}$	$1.99 \times 10^{-6}$
	Big $H_0$	$5.50 \times 10^{-6}$	$5.60 \times 10^{-6}$	$2.22 \times 10^{-6}$	$2.03 \times 10^{-6}$
	Big $H_0$	$3.80 \times 10^{-6}$	$5.20 \times 10^{-6}$	$2.12 \times 10^{-6}$	$1.98 \times 10^{-6}$
Arithmetic mean		$4.10 \times 10^{-6}$	$4.98 \times 10^{-6}$	$2.11 \times 10^{-6}$	$2.10 \times 10^{-6}$
Standard deviation		$6.90 \times 10^{-7}$	$6.49 \times 10^{-7}$	$1.16 \times 10^{-7}$	$2.86 \times 10^{-7}$

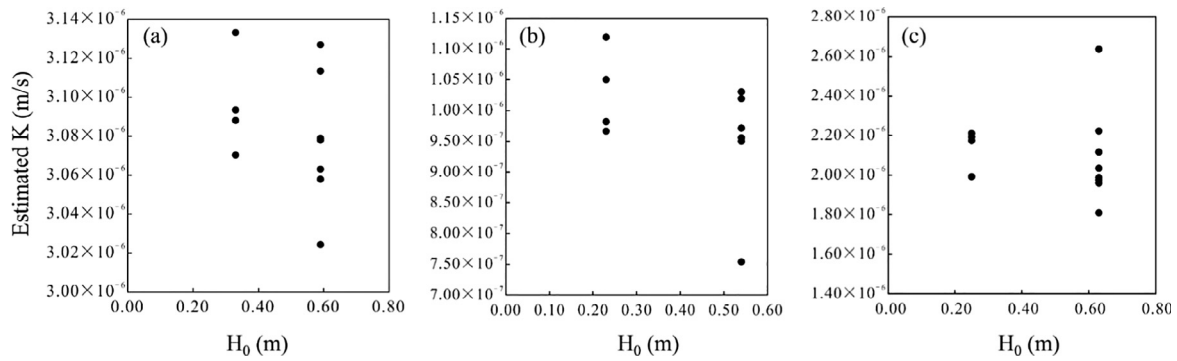


Fig. 7. Relation between the estimated  $K_h$  and  $H_0$  for BW5 (a), BW6 (b) and BW7 (c), respectively. Note difference in vertical scales between subplots.

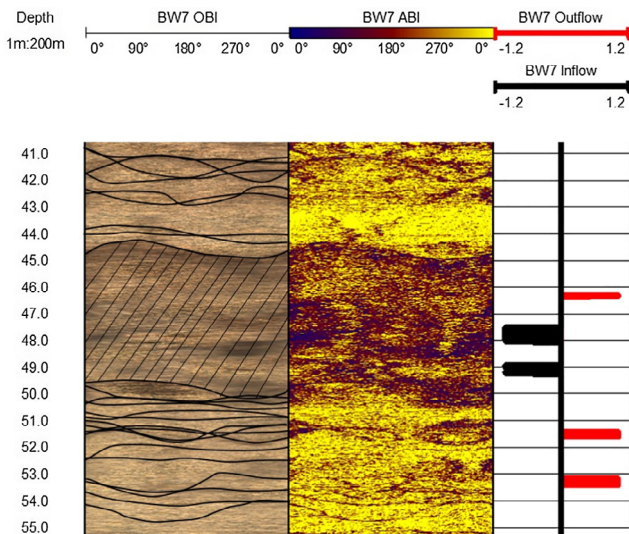


Fig. 8. An example of a flowing fractured zone identified by jointly interpreting borehole televiewer and flowmeter logs in BW7 between 41 and 55 m bgs. Note that the flowing fractured zones (black and red zones) are identified as the intervals where flowmeter logged inflow or outflow rate is greater than  $3.15 \times 10^{-5} \text{ (m}^3/\text{s)}$ .

$$\alpha = \frac{r_s^2 S_s L}{r_c^2} \tag{9}$$

where  $r_s$  is the effective radius of the screen or open borehole [L],  $S_s$  is specific storage [1/L],  $L$  is the length of the open borehole [L], and  $r_c$  is radius of casing [L]. Using the Cooper et al. (1967) model (which yields  $S_s$ ),  $\alpha$  obtained for BW5, 6, and 7 ranges from  $10^{-7}$  to  $10^{-10}$ , which suggests that this deviation is expected and results obtained using Cooper et al. model are less reliable. In the rest of this paper, all  $K_h$  were obtained using the Bouwer–Rice model.

#### 4.1.2. Non-Darcian flow

For moderately permeable fractured dolostone and sandstone with  $K_h$  ranging from  $10^{-4}$ – $10^{-5}$  m/s, Quinn et al. (2013) conducted a series of slug tests as well as constant-head step tests using straddle packers. Their results suggest that non-Darcian flow can be generated under small  $H_0$  ( $\sim 0.2$  m). For a fractured granite with  $K_h$  ranging from  $10^{-7}$ – $10^{-8}$  m/s, however, Ji and Koh (2015) found that nonlinear flow arose only when  $H_0$  was over 1.0 m. A threshold  $H_0$  above which groundwater flow regime transforms to non-Darcian flow thus appears to depend on  $K_h$  of the formation in the vicinity of the well. At BW5, 6, and 7, most  $K_h$  range from  $10^{-6}$ – $10^{-7}$  m/s, which lie in between those of the above reported sites. Thus, non-Darcian flow is evaluated by examining the slug test results. For BW 5, 6, and 7, we examine whether the estimated  $K_h$  depends on the initial slug size. Only BW6 showed that

the mean of the estimated  $K_h$  slightly decreased with increasing  $H_0$  (Fig. 7), although the sample size is small and the lowest estimate ( $7.54 \times 10^{-7}$ ) has strongly influenced this mean. We conclude that non-Darcian flow may have occurred in BW6, while BW5 and BW7 are interpreted to have had only linear flow during slug tests.

To examine potential non-Darcian flow during the slug tests at BW6, a set of Reynolds number ( $Re$ ) were calculated following Ji and Koh (2015), using the monitored hydraulic heads and the estimated number of flowing fractures. Total fracture densities were initially estimated at 0.25 m intervals from the optical (OBI) and acoustic (ABI) logs. The subset of flowing fractures were then identified by a joint analysis of borehole televiewer and constant-rate impeller flowmeter data. The constant rate data were collected when the flowmeter was run both up and down the borehole at the slowest speed possible (1.5 m/min in our case). After correction for the speed and conversion to flow rate (based on previous calibration of the tool in boreholes with known diameters), the upgoing and downgoing flowmeter data were differenced. This results in an impeller flowmeter curve that can be used to highlight zones of inflow and outflow. For the depth interval of 41–55 m bgs in BW7, the OBI and ABI televiewer logs are shown along with the impeller flowmeter log (Fig. 8). The black and red zones displayed in the filtered flowmeter log represent inflow and outflow, respectively, for this fracture zone. Only the depth intervals that correspond to inflow (black) and outflow (red) zones are then considered as flowing fracture zones. For all three wells, the number of fractures identified from borehole televiewer logs is plotted along with the number of flowing fractures as additionally filtered by borehole flowmeter (Fig. 9). The total number of flowing fractures determined at BW5, BW6, and BW7, at 1.0 m intervals, are 143, 113, and 174, respectively.

For BW6, Fig. 10 shows the calculated  $Re$  for every second of a slug test. This  $Re$  was also compared among the slug tests with different  $H_0$  at this well. The maximum  $Re$  calculated from a set of tests (i.e., five FH tests and five RH tests) are always under 8, and most of the  $Re$  are under 3.  $Re$  computed for the two different  $H_0$  also do not differ significantly. In addition, there are no trends indicating that the larger  $H_0$  results in a larger early-time  $Re$  nor that a larger early-time  $Re$  corresponds to smaller estimated  $K_h$  (Fig. 11). In summary, for all three wells, groundwater flow during the slug tests using the small  $H_0$  (i.e., 0.23 m) are always in linear flow regime. For the slug tests carried out using the larger  $H_0$ , non-Darcian flow is nonexistent or negligible.

#### 4.2. Flute profiling results and analysis

For the three wells, borehole  $K_h$  determined using FLUTE blank profiling is shown in Fig. 12. For all wells, the  $K_h$  profiles, i.e., a discrete  $K_h$  value determined over  $\sim 30$  cm borehole interval, exhibit a decreasing trend with depth which corresponds to the observed decrease in the frequency of flowing fractures with depth as obtained from flowmeter logging (see Fig. 9). At each well, the  $K_h$  profile exhibits variation over  $\sim 4$  orders of magnitude, with maximum  $K_h$  reaching up

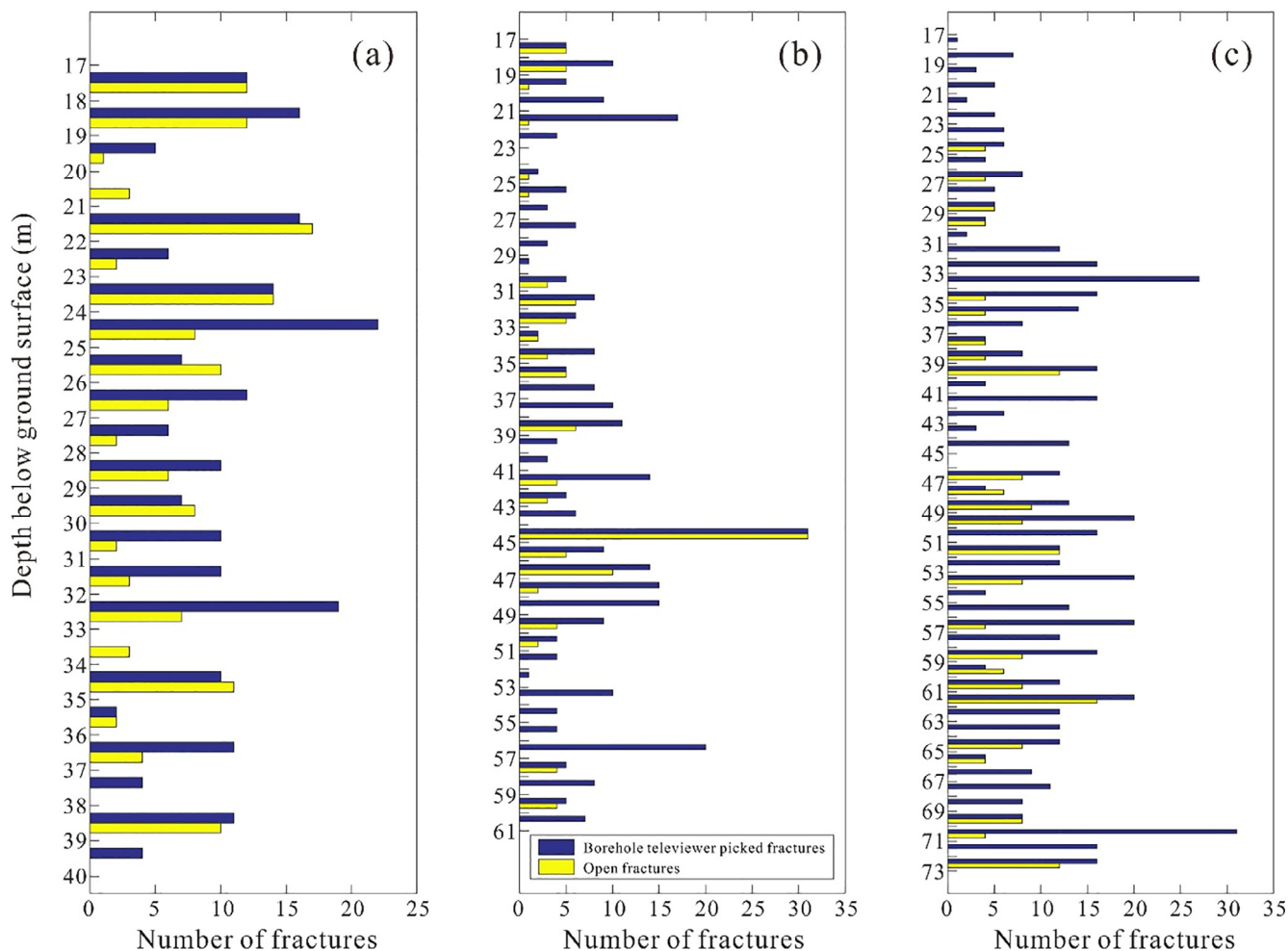


Fig. 9. Fracture density picked from borehole televiewer and flowing fractures filtered by borehole flowmeter logging for BW5 (a), BW6 (b), and BW7(c), respectively. Topographic elevation of the ground above sea level at each borehole is 2487.16 m for BW5, 2475.63 m for BW6, and 2475.43 m for BW7.

to  $10^{-5}$  m/s. Despite the variability,  $K_h$  values are consistently higher near the top of the open borehole. Clearly, significant vertical heterogeneity exists in this aquifer, whereas  $K_h$  is the highest at the top of the bedrock. This region lies beneath the saprolite zone which receives snow water infiltration from the land surface. The top of the fractured bedrock thus lies at the so called weathering front (Flinchum, 2017). However, the formulation used to determine the FLUTE  $K_h$  profile is deterministic (in the field, transducer measurement errors were considered relatively insignificant). Further analysis may be required to determine the uncertainty in the estimation, although for all wells, the FLUTE determined  $K_h$  profiles yield an equivalent open hole transmissivity that is similar in magnitude (and often much better, within a factor of 2) with those determined by the slug tests (Table 3). It is noteworthy that the FLUTE values for BW5 and 6 are just above the upper end of the slug test ranges, but that for BW7, is below the slug test range.  $K_h$  estimated at the upper portion of the borehole can be less reliable because the transmissivity over the remaining borehole interval is relatively high, which gives rise to a faster liner descent velocity (Quinn et al., 2015). Since the detection limit of FLUTE liner profiling is a function of the descent velocity, and small velocity changes can be difficult to detect if the descent velocity is high, the FLUTE method may underestimate the high  $K_h$  intervals during the early profiling period (i.e., two notable peak values in the BW7 FLUTE interval). Moreover, FLUTE profiling was done months before the slug tests, and near-bore fractures may have changed over this time due to fines migration and settling. All these factors can influence the estimated  $K_h$  between slug tests and FLUTE profiling. Without further testing, it is difficult to

determine why the FLUTE values for BW5 and 6 are just above the upper end of the slug test ranges, but that for BW7, is below the slug test range. Overall, FLUTE determined  $K_h$  profiles yield an equivalent open hole transmissivity similar to those determined by the slug tests.

#### 4.3. Determination of hydraulic aperture and groundwater velocity

Using the number of flowing fractures as determined from borehole televiewer and flowmeter logs and the transmissivity values obtained from slug tests and FLUTE, an average hydraulic aperture for a given tested interval (i.e., vertical resolution in FLUTE profiles or the entire open borehole tested by a slug test) can be obtained using Eq. (8). For all three wells, the distribution of  $b$  based on FLUTE profiling is shown along with its univariate statistics (Fig. 13). In the same figure,  $b$  determined based on the mean  $K_h$  value obtained from the slug tests is also shown. Because the slug-test-derived  $K_h$  varies over a narrow range (the standard deviation is generally less than  $10^{-7}$  m/s) with fewer measurements, a distribution of slug-test-derived  $b$  is not presented. Results suggest that, for all three wells, (1) the FLUTE-derived- $b$  varies greatly at each well, indicating substantial vertical variability in the distribution of fracture aperture; (2) there is lateral variability in the mean hydraulic aperture obtained from both the FLUTE and slug tests:  $b$  for BW5, BW6, and BW7 is 90/92  $\mu\text{m}$ , 88/86  $\mu\text{m}$ , and 103/105  $\mu\text{m}$ , respectively (Table 4 and Fig. 13); (3) a high degree of correspondence exists between the average  $b$  derived from FLUTE profiling and the  $b$  value determined from slug tests, which confirms a similar scaling relation observed between slug-tests-derived transmissivity and those of

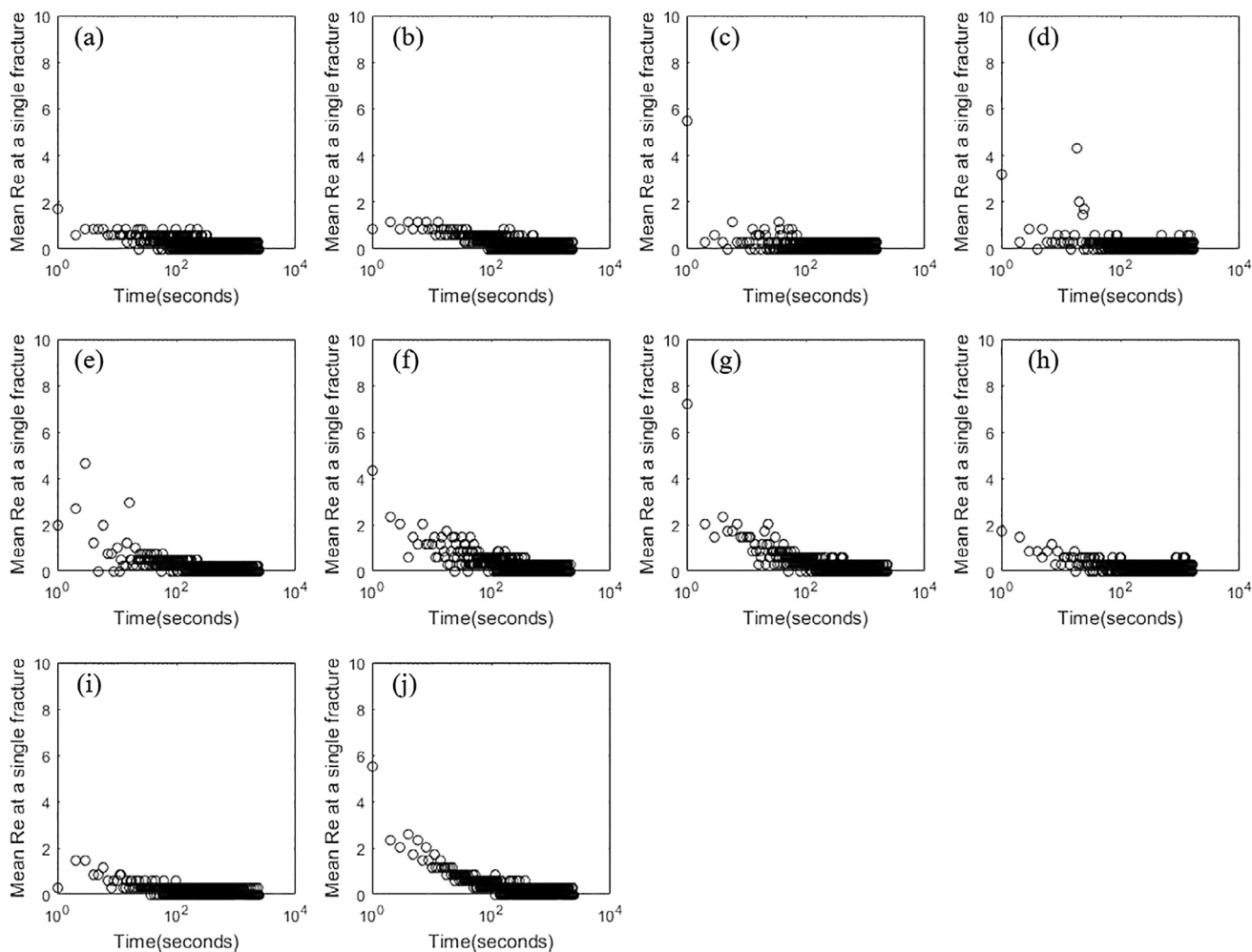


Fig. 10. Calculated mean Re at flowing fracture during slug tests for BW6. (a), (b), (c), (d), and (e) are calculated from the FH tests; (f), (g), (h), (i) and (j) are calculated from the RH tests. (a), (b), (e), (f), (g) and (j) are calculated from large  $H_0 = 0.54$  m, while (c), (d), (h) and (i) are calculated from small  $H_0 = 0.23$  m.

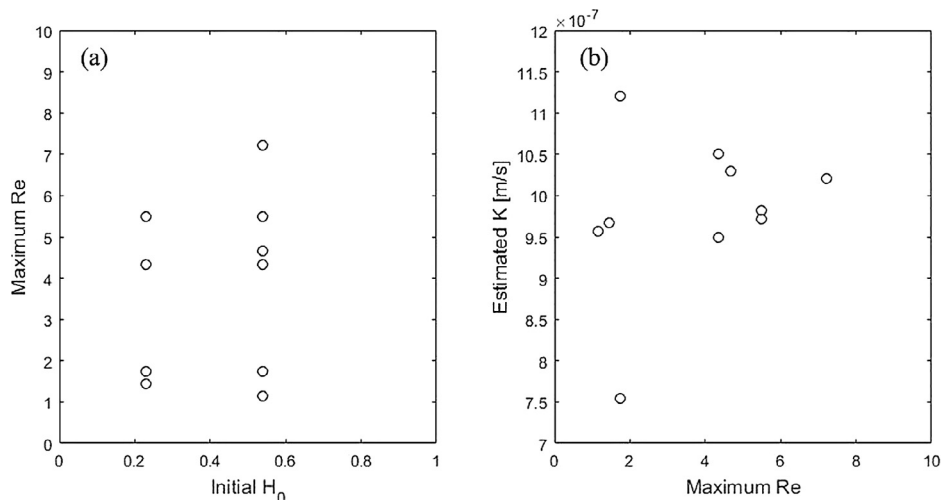


Fig. 11. (a) Relation between  $H_0$  and maximum Re during slug tests at borehole BW6. (b) Relation between maximum Re and the estimated  $K_f$  for each slug tests at borehole BW6.

multilevel injection tests for a fractured granite aquifer in Mirror Lake, New Hampshire (Shapiro and Hsieh, 1998). Therefore, at this site, slug test can be used to estimate an accurate average hydraulic aperture over the open hole. If the distribution of hydraulic aperture is required, high resolution  $T$  data along the open hole is needed.

There are two conceptual approaches for determining groundwater velocity, one is the equivalent porous media (EPM) model (Freeze and Cherry, 1979) and the other is the discrete fracture parallel-plate model (Novakowski, 2000). Both models emphasize laminar flow upon which the Darcy law is established. In the EPM model, the formation is

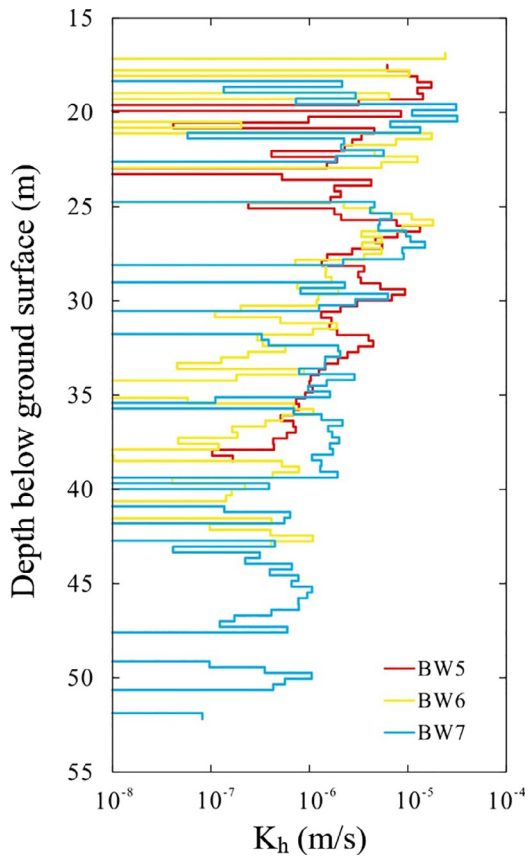


Fig. 12. Results of FLUTE  $K_h$  profiles for the open holes of BW5, BW6, and BW7.

**Table 3**  
Comparison of calculated transmissivity for the open borehole based on slug tests and FLUTE profiling at each well.

Well	Slug test $T$ ( $m^2/s$ )	FLUTE profiling $T$ ( $m^2/s$ )
BW5	$6.36 \times 10^{-5} \sim 6.59 \times 10^{-5}$	$7.42 \times 10^{-5}$
BW6	$3.30 \times 10^{-5} \sim 4.89 \times 10^{-5}$	$5.90 \times 10^{-5}$
BW7	$1.01 \times 10^{-4} \sim 1.47 \times 10^{-4}$	$8.31 \times 10^{-5}$

analyzed by treating it as an equivalent homogeneous porous medium. In the discrete fracture model, all flow is assumed to occur in the interconnected fractures and rock matrix is considered impermeable.

**Table 4**  
Transmissivity and average hydraulic aperture estimated from slug test results at each of the three borehole.

Well	Test Sequence	Transmissivity ( $m^2/s$ )		Average hydraulic aperture ( $\mu m$ )		Number of flowing fractures along the open hole		
		FH	RH	FH	RH			
BW5	Big $H_o$	$6.36 \times 10^{-5}$	$3.11 \times 10^{-6}$	91	92	143		
	Big $H_o$	$6.47 \times 10^{-5}$	$3.06 \times 10^{-6}$	92	92			
	Small $H_o$	$6.49 \times 10^{-5}$	$3.09 \times 10^{-6}$	92	91			
	Small $H_o$	$6.45 \times 10^{-5}$	$3.13 \times 10^{-6}$	92	92			
	Big $H_o$	$6.47 \times 10^{-5}$	$3.08 \times 10^{-6}$	92	92			
	Big $H_o$	$6.57 \times 10^{-5}$	$3.06 \times 10^{-6}$	92	92			
Arithmetic mean								
Standard deviation		$6.93 \times 10^{-7}$	$6.56 \times 10^{-8}$	0.37	0.37			
BW6	Big $H_o$	$3.30 \times 10^{-5}$	$4.15 \times 10^{-5}$	79	86	113		
	Big $H_o$	$4.18 \times 10^{-5}$	$4.46 \times 10^{-5}$	86	88			
	Small $H_o$	$4.29 \times 10^{-5}$	$4.89 \times 10^{-5}$	87	91			
	Small $H_o$	$4.59 \times 10^{-5}$	$4.22 \times 10^{-5}$	89	86			
	Big $H_o$	$4.50 \times 10^{-5}$	$4.24 \times 10^{-5}$	88	86			
	Big $H_o$	$4.17 \times 10^{-5}$	$4.39 \times 10^{-5}$	86	87			
Arithmetic mean								
Standard deviation		$4.62 \times 10^{-6}$	$2.69 \times 10^{-6}$	3.55	1.97			
BW7	Big $H_o$	$1.11 \times 10^{-4}$	$1.47 \times 10^{-4}$	103	113	174		
	Big $H_o$	$1.09 \times 10^{-4}$	$1.01 \times 10^{-4}$	102	100			
	Small $H_o$	$1.22 \times 10^{-4}$	$1.21 \times 10^{-4}$	106	106			
	Small $H_o$	$1.23 \times 10^{-4}$	$1.11 \times 10^{-4}$	107	103			
	Big $H_o$	$1.24 \times 10^{-4}$	$1.13 \times 10^{-4}$	107	104			
	Big $H_o$	$1.18 \times 10^{-4}$	$1.10 \times 10^{-4}$	105	103			
	Big $H_o$	$1.18 \times 10^{-4}$	$1.17 \times 10^{-4}$	105	105			
	Arithmetic mean							
	Standard deviation		$6.45 \times 10^{-6}$	$1.60 \times 10^{-5}$	1.92		4.06	

Note: Water density  $\rho_w = 1000 \text{ kg/m}^3$ , and dynamic viscosity  $\mu = 1.4 \times 10^{-3} \text{ kg/m}\cdot\text{s}$  are referred from Table 2.1, Fitts (2002).

Under the assumption that all the flowing fractures are identical with the same local  $T$  values, both methods will result in the same computed average linear groundwater velocity ( $v$ ). Below, we assume that, for each interval analyzed by the slug test or FLUTE profiling, it contains an

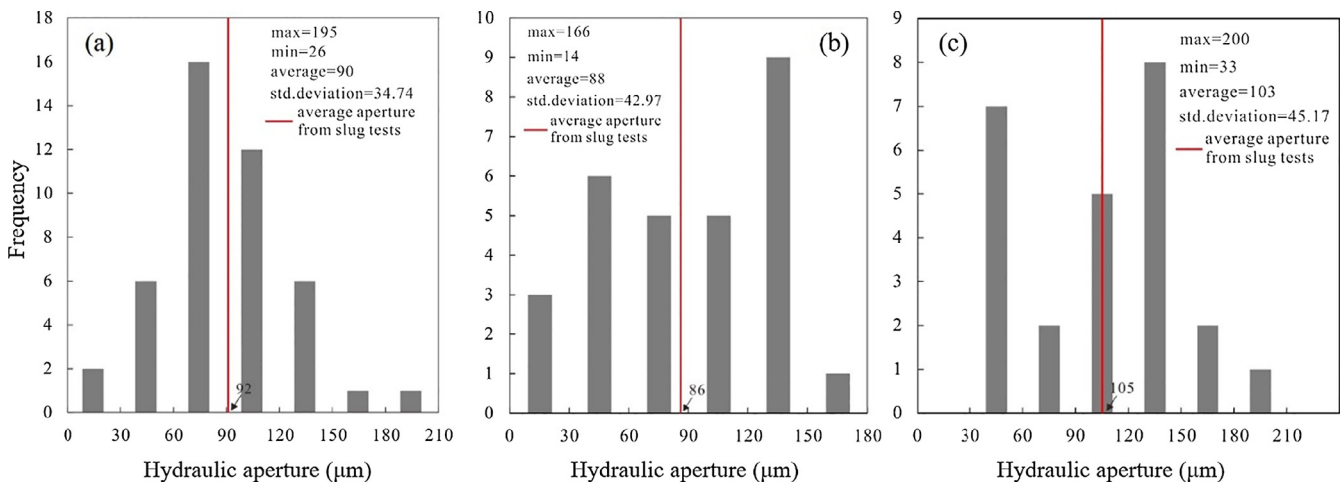
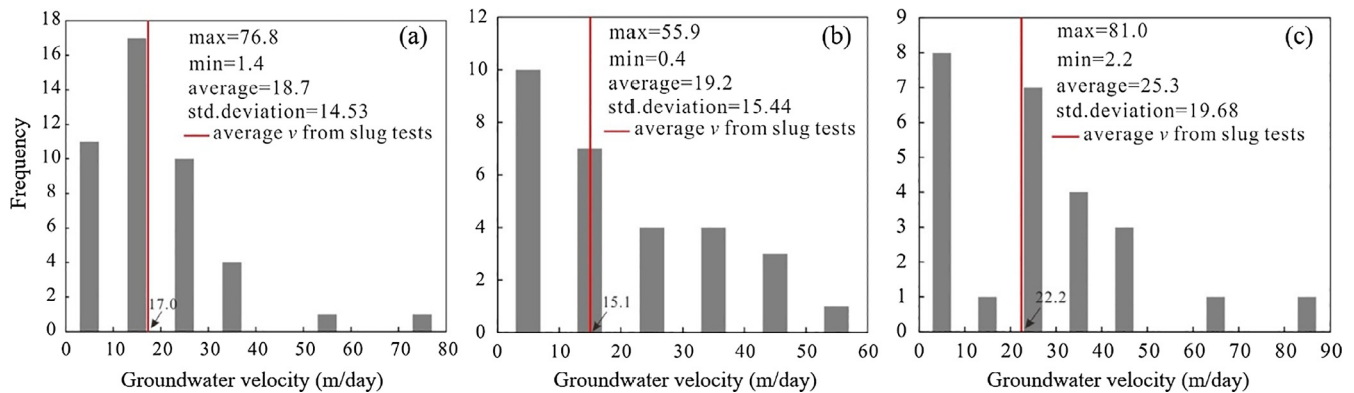


Fig. 13. Distribution of hydraulic aperture derived from the FLUTE profiles and comparison with the mean value of hydraulic aperture calculated from slug tests (red line) for BW5 (a), BW6 (b), and BW7 (c), respectively.

**Table 5**  
Groundwater velocity calculation using an equivalent porous media (EPM) model from slug test results for the three boreholes.

Well	Test Sequence	K (m/s)		dh/dx	q <sub>h</sub> (m/s)		ϕ <sub>f</sub>		v (m/day)	
		FH	RH		FH	RH	FH	RH	FH	RH
BW5	Big H <sub>0</sub>	3.02 × 10 <sup>-6</sup>	3.11 × 10 <sup>-6</sup>	0.04	1.21 × 10 <sup>-7</sup>	1.25 × 10 <sup>-7</sup>	6.2 × 10 <sup>-4</sup>	6.3 × 10 <sup>-4</sup>	16.8	17.2
	Big H <sub>0</sub>	3.08 × 10 <sup>-6</sup>	3.06 × 10 <sup>-6</sup>	0.04	1.23 × 10 <sup>-7</sup>	1.22 × 10 <sup>-7</sup>	6.2 × 10 <sup>-4</sup>	6.2 × 10 <sup>-4</sup>	17.0	17.0
	Small H <sub>0</sub>	3.09 × 10 <sup>-6</sup>	3.09 × 10 <sup>-6</sup>	0.04	1.24 × 10 <sup>-7</sup>	1.24 × 10 <sup>-7</sup>	6.3 × 10 <sup>-4</sup>	6.3 × 10 <sup>-4</sup>	17.1	17.1
	Small H <sub>0</sub>	3.07 × 10 <sup>-6</sup>	3.13 × 10 <sup>-6</sup>	0.04	1.23 × 10 <sup>-7</sup>	1.25 × 10 <sup>-7</sup>	6.2 × 10 <sup>-4</sup>	6.3 × 10 <sup>-4</sup>	17.0	17.2
	Big H <sub>0</sub>	3.08 × 10 <sup>-6</sup>	3.08 × 10 <sup>-6</sup>	0.04	1.23 × 10 <sup>-7</sup>	1.23 × 10 <sup>-7</sup>	6.2 × 10 <sup>-4</sup>	6.2 × 10 <sup>-4</sup>	17.0	17.0
	Big H <sub>0</sub>	3.13 × 10 <sup>-6</sup>	3.06 × 10 <sup>-6</sup>	0.04	1.25 × 10 <sup>-7</sup>	1.23 × 10 <sup>-7</sup>	6.3 × 10 <sup>-4</sup>	6.2 × 10 <sup>-4</sup>	17.2	17.0
Arithmetic mean		3.08 × 10 <sup>-6</sup>	3.09 × 10 <sup>-6</sup>		1.23 × 10 <sup>-7</sup>	1.24 × 10 <sup>-7</sup>	6.2 × 10 <sup>-4</sup>	6.2 × 10 <sup>-4</sup>	17.0	17.1
Standard deviation		3.31 × 10 <sup>-8</sup>	2.93 × 10 <sup>-8</sup>		1.32 × 10 <sup>-9</sup>	1.18 × 10 <sup>-9</sup>	5.73 × 10 <sup>-6</sup>	6.50 × 10 <sup>-6</sup>	0.12	0.11
BW6	Big H <sub>0</sub>	7.54 × 10 <sup>-7</sup>	9.50 × 10 <sup>-7</sup>	0.04	3.02 × 10 <sup>-8</sup>	3.80 × 10 <sup>-8</sup>	2.1 × 10 <sup>-4</sup>	2.2 × 10 <sup>-4</sup>	12.7	14.8
	Big H <sub>0</sub>	9.56 × 10 <sup>-7</sup>	1.02 × 10 <sup>-6</sup>	0.04	3.82 × 10 <sup>-8</sup>	4.08 × 10 <sup>-8</sup>	2.2 × 10 <sup>-4</sup>	2.3 × 10 <sup>-4</sup>	14.9	15.5
	Small H <sub>0</sub>	9.82 × 10 <sup>-7</sup>	1.12 × 10 <sup>-6</sup>	0.04	3.93 × 10 <sup>-8</sup>	4.48 × 10 <sup>-8</sup>	2.2 × 10 <sup>-4</sup>	2.3 × 10 <sup>-4</sup>	15.1	16.5
	Small H <sub>0</sub>	1.05 × 10 <sup>-6</sup>	9.67 × 10 <sup>-7</sup>	0.04	4.20 × 10 <sup>-8</sup>	3.87 × 10 <sup>-8</sup>	2.3 × 10 <sup>-4</sup>	2.2 × 10 <sup>-4</sup>	15.8	15.0
	Big H <sub>0</sub>	1.03 × 10 <sup>-6</sup>	9.72 × 10 <sup>-7</sup>	0.04	4.12 × 10 <sup>-8</sup>	3.89 × 10 <sup>-8</sup>	2.3 × 10 <sup>-4</sup>	2.2 × 10 <sup>-4</sup>	15.6	15.0
	Big H <sub>0</sub>	9.55 × 10 <sup>-7</sup>	1.01 × 10 <sup>-6</sup>		3.82 × 10 <sup>-8</sup>	4.02 × 10 <sup>-8</sup>	2.2 × 10 <sup>-4</sup>	2.3 × 10 <sup>-4</sup>	14.8	15.4
Arithmetic mean		9.55 × 10 <sup>-7</sup>	1.01 × 10 <sup>-6</sup>		3.82 × 10 <sup>-8</sup>	4.02 × 10 <sup>-8</sup>	2.2 × 10 <sup>-4</sup>	2.3 × 10 <sup>-4</sup>	14.8	15.4
Standard deviation		1.06 × 10 <sup>-7</sup>	6.16 × 10 <sup>-8</sup>		4.72 × 10 <sup>-9</sup>	2.75 × 10 <sup>-9</sup>	9.78 × 10 <sup>-6</sup>	6.93 × 10 <sup>-6</sup>	1.26	0.70
BW7	Big H <sub>0</sub>	1.99 × 10 <sup>-6</sup>	2.64 × 10 <sup>-6</sup>	0.04	7.95 × 10 <sup>-8</sup>	1.05 × 10 <sup>-7</sup>	3.2 × 10 <sup>-4</sup>	3.5 × 10 <sup>-4</sup>	21.4	25.8
	Big H <sub>0</sub>	1.96 × 10 <sup>-6</sup>	1.81 × 10 <sup>-6</sup>	0.04	7.84 × 10 <sup>-8</sup>	7.24 × 10 <sup>-8</sup>	3.2 × 10 <sup>-4</sup>	3.1 × 10 <sup>-4</sup>	21.2	20.1
	Small H <sub>0</sub>	2.19 × 10 <sup>-6</sup>	2.17 × 10 <sup>-6</sup>	0.04	8.77 × 10 <sup>-8</sup>	8.70 × 10 <sup>-8</sup>	3.3 × 10 <sup>-4</sup>	3.3 × 10 <sup>-4</sup>	22.8	22.7
	Small H <sub>0</sub>	2.21 × 10 <sup>-6</sup>	1.99 × 10 <sup>-6</sup>	0.04	8.84 × 10 <sup>-8</sup>	7.97 × 10 <sup>-8</sup>	3.3 × 10 <sup>-4</sup>	3.2 × 10 <sup>-4</sup>	23.0	21.4
	Big H <sub>0</sub>	2.22 × 10 <sup>-6</sup>	2.03 × 10 <sup>-6</sup>	0.04	8.89 × 10 <sup>-8</sup>	8.14 × 10 <sup>-8</sup>	3.3 × 10 <sup>-4</sup>	3.2 × 10 <sup>-4</sup>	23.0	21.7
	Big H <sub>0</sub>	2.12 × 10 <sup>-6</sup>	1.98 × 10 <sup>-6</sup>	0.04	8.47 × 10 <sup>-8</sup>	7.90 × 10 <sup>-8</sup>	3.3 × 10 <sup>-4</sup>	3.2 × 10 <sup>-4</sup>	22.3	21.3
Arithmetic mean		2.11 × 10 <sup>-6</sup>	2.10 × 10 <sup>-6</sup>		8.46 × 10 <sup>-8</sup>	8.42 × 10 <sup>-8</sup>	3.3 × 10 <sup>-4</sup>	3.3 × 10 <sup>-4</sup>	22.3	22.2
Standard deviation		1.16 × 10 <sup>-7</sup>	2.86 × 10 <sup>-7</sup>		4.63 × 10 <sup>-9</sup>	1.15 × 10 <sup>-8</sup>	6.48 × 10 <sup>-6</sup>	1.47 × 10 <sup>-5</sup>	0.82	1.97



**Fig. 14.** Distribution of groundwater velocity derived from FLUTE profiles and the mean value of groundwater velocity calculated from the slug test results (red line) for BW5 (a), BW6 (b), and BW7 (c), respectively.

identical set of horizontal flowing fractures. Thus, assuming an EPM,  $v$  is computed using a field scale Darcy flux [L/T] and an effective fracture porosity ( $\phi_f$ ):

$$v = \frac{q_h}{\phi_f}; q_h = K_h \frac{dh}{dx} \tag{10}$$

where  $\phi_f$  [-] is determined using the estimated hydraulic aperture(s) for the fracture(s) divided by the length of open hole and  $\frac{dh}{dx}$  [-] is the lateral hydraulic gradient along the direction of the flow, which was computed based on long term water level observations. An average hydraulic gradient of 0.04 was used to calculate Darcy flux for both slug tests and FLUTE liner profile.

Based on data collected at all three wells, an estimated effective or bulk  $\phi_f$  is on the order of  $10^{-4}$ , which is within the range for fractured rock ( $10^{-2}$ – $10^{-5}$ ) as reported by Freeze and Cherry (1979) with a standard deviation on the order of  $10^{-6}$  (Table 5). A set of computed groundwater velocities obtained based on slug test results are also listed. The average groundwater velocity calculated based on slug tests is 17.0 m/day (BW5), 15.1 m/day (BW6), and 22.2 m/day (BW7), respectively. In addition, for the same wells, an average  $v$  for each interval of the FLUTE profile can be obtained using Eq. (10) assuming a

homogeneous equivalent porous medium (Fig. 14). Similar to the estimated hydraulic aperture along the open hole, groundwater velocity exhibits ~2 orders of magnitude variation at each well, with a minimum of 0.4 m/day and a maximum value of 81.0 m/day. This corresponds to the heterogeneity of the FLUTE-derived  $K_h$ . The calculated groundwater velocity is similar to the results reported by Quinn et al. (2011a,b) for a fractured dolostone aquifer. It should also be pointed out that from Eqs. (8) and (10), one can deduce that for each FLUTE test interval:

$$v = \frac{T}{bN} \frac{dh}{dx} \tag{11}$$

This indicates that groundwater velocity distribution is related to three distributions:  $b$ ,  $N$ , and  $T$ . Thus, the  $v$  histogram does not have a linear correlation with the  $b$  histogram.

#### 4.4. Geological model of Blair Wallis

Based on all available site data, including cores, borehole logs, LIDAR topography, and a seismic P-wave velocity model, three zones can be identified at the well field: upper saprolite, middle fractured

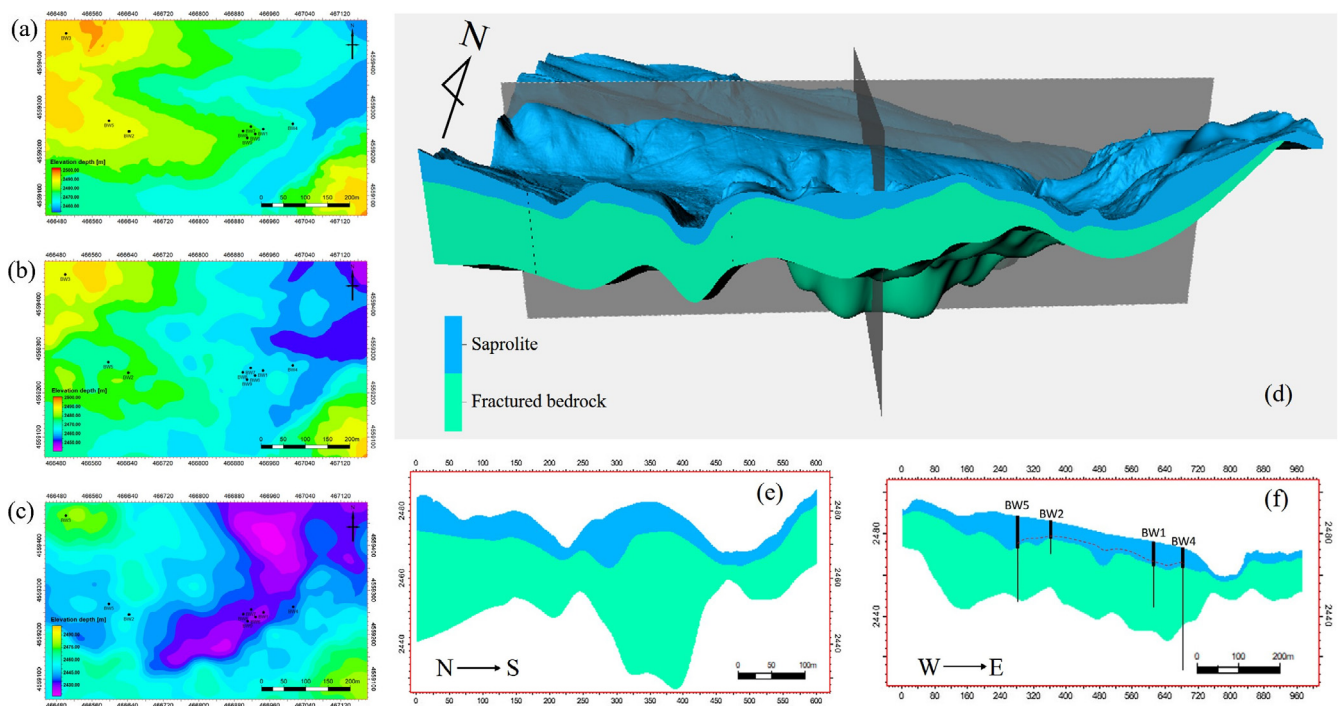


**Fig. 15.** (a) LIDAR topography of Blair Wallis well field. (b) Interpreted interface between saprolite and fractured granite by extracting the 1.2 km/s P-wave velocity contour from a kriged volume (Flinchum, 2017). (c) Interpreted interface between fractured granite and less fractured protolith by extracting the 4.0 km/s surface (Flinchum, 2017). (d) A geological model of the well field (vertically exaggerated 4 times) based on (a), (b), (c). (e) A N-S cross section through (d), which intersects 4 boreholes (for each borehole, the surface casing is marked by a thick vertical line, and the total depth of the borehole is marked by a thin vertical line). The dashed line is the long-term average water table interpolated from well water levels.

bedrock, and underlying protolith (less fractured bedrock). The saprolite and fractured bedrock boundary was first determined at the borehole location at approximately the bottom of the surface casing. Flinchum (2017) identified a 1.2 km/s seismic P-wave velocity associated with that depth and created this boundary by extracting the 1.2 km/s velocity contour map from a three-dimensional (3D) volume of the inverted P-wave velocities. According to Flinchum (2017), the boundary between fractured granite and protolith is estimated by extracting the 4.0 km/s velocity contour map from the same 3D volume, because this velocity was estimated by conducting a survey over an intact granite outcrop near the well field. For the upper two zones, a 3D geological model of the field site was built (Fig. 15), where the fractured bedrock is observed to be  $\sim 4\times$  the thickness of the saprolite. Along an East-West cross section of the model (Fig. 15(f)), which parallels the average hydraulic head gradient, long-term average water levels from four wells are projected. Despite the limited data, water levels appear to be following the boundary between the saprolite and fractured bedrock. The water levels were thus interpolated between the wells following the same boundary. Despite local variations, water table dips to the east and suggests topographically driven flow.

## 5. Conclusions

In this study, hydraulic parameters of an unconfined fractured granite aquifer were characterized using borehole data from three wells in the Blair Wallis Fractured Rock Hydrology Research Well field in Laramie Range, Wyoming. The borehole data include those from hydraulic tests (i.e., slug tests and FLUTE profiling) and borehole logging (i.e., flowmeter under ambient flow condition, optical, and acoustic televiwer). By analyzing a set of repeat slug tests with different initial displacements and calculating an average  $Re$  for either individual or equivalent fracture, we concluded that both skin effect and non-Darcian flow, which may lead to an underestimated horizontal hydraulic conductivity ( $K_h$ ), are negligible during the slug tests. FLUTE profiling, a

high-resolution  $K_h$  profiling method (at the research site, it has  $\sim 0.3$  m vertical resolution) was used as an alternative way of estimating discrete  $K_h$ . By jointly interpreting borehole televiwer logs with flowmeter logs, the number of flowing fractures along the open borehole can be determined for each well. Based on  $K_h$  estimates from slug tests and FLUTE, an average hydraulic aperture is estimated for the entire open hole and for the discrete FLUTE test intervals. Given the aperture data and the site-scale horizontal hydraulic gradient, an effective fracture porosity and groundwater velocity were estimated. Finally, based on all available data, including cores, borehole logs, LIDAR topography, and a seismic P-wave velocity model, a three dimensional geological model of the site was built. Results of this characterization study are summarized as:

- (1) a hydraulically significant zone at the well field extends to  $\sim 40$ – $53$  m depth. Based on FLUTE profiling,  $K_h$  of the three wells varies over  $\sim 4$  orders of magnitude ( $10^{-8}$ – $10^{-5}$  m/s), with a maximum value reaching  $10^{-5}$  m/s. Despite this variability,  $K_h$  is found to be consistently higher near the top of the open holes compared to  $K_h$  of the deeper intervals. This high- $K$  zone corresponds to observed high fracture density in the bedrock, which is interrelated by us to be the weathering front.
- (2) The FLUTE-estimated hydraulic apertures for all wells vary over one order of magnitude ( $14\ \mu\text{m}$  –  $200\ \mu\text{m}$ ), indicating vertical heterogeneity in fractures. Based on slug test derived  $K_h$ , average hydraulic apertures calculated are  $92\ \mu\text{m}$  (BW5),  $86\ \mu\text{m}$  (BW6), and  $105\ \mu\text{m}$  (BW7). Moreover, at each well, an average aperture obtained from its FLUTE profile is very close to that obtained from slug test, suggesting that slug test can be used to provide a reliable average aperture estimate.
- (3) Based on the estimated hydraulic apertures, an effective fracture porosity is estimated to be  $4.0 \times 10^{-4}$  with a standard deviation of  $8.4 \times 10^{-6}$ , thus fractured crystalline rock in this headwater watershed can host significant quantity of groundwater.

- (4) Given water level monitoring data, which suggest an average hydraulic gradient of 0.04 under ambient flow condition, groundwater velocity is estimated to range from 0.4 to 81.0 m/day, implying rapid pathways for groundwater flow. However, these values are considered a rough approximation because only a single gradient value in space/time is used. Under other flow conditions, especially following spring snowmelt which occurred before the well test season, groundwater velocity is likely different with more significant flow.
- (5) The average ambient water table position follows the interface between saprolite and fractured bedrock and dips to the east. The groundwater system at the site appears to be topography driven.

Because groundwater flow in crystalline rocks not only depends on fracture aperture and porosity, but also depends on the connectivity of the fractures, future work will aim to characterize the orientation, extent, and connectivity of the fracture network at the well field by employing cross-hole hydraulic tests in combination with surface and borehole geophysical measurements. Depending on the specific geophysical and hydraulic testing methods, however, increased volumes of the fractured aquifer will likely be interrogated, e.g., laterally, such volume can range from the near-wellbore-scale to inter-well or larger scales, and vertically, parameters can be obtained at either logging resolution or for an entire borehole interval. In fractured rocks, “scale effects” is a well-known phenomenon (e.g., Hsieh, 1998; Rovey and Niemann, 2001; Hyun et al., 2002; Neuman and Di Federico, 2003; Illman, 2006; Jazayeri Noushabadi et al., 2011), future work will also evaluate the existence of scale effects.

## Acknowledgments

This well field research is supported by WATER (Cyberinfrastructure to Advance High Performance Water Resource Modeling), and NSF EPSCoR (EPS 1208909). The financial support by International colleges and universities jointly cultivate doctoral program from China University of Geosciences (Wuhan) is greatly acknowledged.

## References

- Bales, R.C., Molotch, N.P., Painter, T.H., Dettinger, M.D., Rice, R., Dozier, J., 2006. Mountain hydrology of the western United States. *Water Resour. Res.* 42, W08432. <http://dx.doi.org/10.1029/2005WR004387>.
- Barnett, T.P., Adam, J.C., Lettenmaier, D.P., 2005. Potential impacts of a warming climate on water availability in snow-dominated regions. *Nature* 438, 303–309. <http://dx.doi.org/10.1038/nature04141>.
- Bouwer, H., Rice, R.C., 1976. A slug test for determining hydraulic conductivity of unconfined aquifers with completely or partially penetrating wells. *Water Resour. Res.* 12 (3), 423–428.
- Butler Jr., J.J., McElwee, C.D., Liu, W., 1996. Improving the quality of parameter estimates obtained from slug tests. *Ground Water* 34 (3), 480–490.
- Butler Jr., J.J., 1998. *The Design, Performance, and Analysis of Slug Tests*. Lewis, London pp. 252.
- Butler Jr., J.J., Dietrich, P., Wittig, V., Christy, T., 2007. Characterizing hydraulic conductivity with the direct-push permeameter. *Ground Water* 45 (4), 409–419.
- Cook, P.G., 2003. *A Guide to Regional Groundwater Flow in Fractured Rock Aquifers*. Seaview Press.
- Cooper, H.H., Bredehoeft, J.D., Papadopoulos, S.S., 1967. Response of a finite diameter well to an instantaneous charge of water. *Water Resour. Res.* 3 (1), 263–269.
- Charles R. Fitts, 2002. *Groundwater Science* (Second Ed.), pp. 22.
- Flinchum, B. A., 2017. *Imaging, Characterizing, and Understanding the Critical Zone: A Near-Surface Geophysical Perspective*, Ph.D. dissertation, Dep. Of Geol. and Geophys., Univ. of Wyoming, Laramie, Wyoming, United States.
- Freeze, R.A., Cherry, J.A., 1979. *Groundwater*. Prentice Hall, Inc.
- Frost, C.D., Frost, B.R., Chamberlain, K.R., Edwards, B.R., 1999. Petrogenesis of the 1.43 Ga Sherman batholith, SE Wyoming, USA: A reduced, rapakivi-type anorogenic granite. *J. Petrol.* 40 (12), 1771–1802. <http://dx.doi.org/10.1093/ptro/40.12.1771>.
- Gustafson, G., Krásný, J., 1994. Crystalline rock aquifers: their occurrence, use and importance. *Appl. Hydrogeol.* 2, 64–75.
- Guihéneuf, N., Boisson, A., Bour, O., Dewandel, B., Perrin, J., Dausse, A., Viossanges, M., Chandra, S., Ahmed, S., Maréchal, J.C., 2014. Groundwater flows in weathered crystalline rocks: impact of piezometric variations and depth dependent fracture connectivity. *J. Hydrol.* 511, 320–334.
- Hood, J.L., Hayashi, M., 2015. Characterization of snowmelt flux and groundwater storage in an alpine headwater basin. *J. Hydrol.* 521, 482–497. <http://dx.doi.org/10.1016/j.jhydrol.2014.12.041>.
- Hsieh, P.A., 1998. Scale effects in fluid flow through fractured geologic media. In: Sposito, G. (Ed.), *Scale Dependence and Scale Invariance in Hydrology*. Cambridge University Press, Cambridge, pp. 335–353.
- Hvorslev, M.J., 1951. Time lag and soil permeability in ground-water observations. *Waterways Exper. Sta. Corps of Engrs., US Army* 36.
- Hyder, Z., Butler Jr, J.J., 1995. Slug tests in unconfined formations: an assessment of the Bouwer and Rice technique. *Ground Water* 33 (1), 16–22.
- Hyder, Z., Butler Jr., J.J., McElwee, C.D., Liu, W.Z., 1994. Slug tests in partially penetrating wells. *Water Resour. Res.* 30 (11), 2945–2958.
- Hyun, Y., Neuman, S.P., Vesselinov, V.V., Illman, W.A., Tartakovsky, D.M., Di Federico, V., 2002. Theoretical interpretation of a pronounced permeability scale-effect in unsaturated fractured tuff. *Water Resour. Res.* 38 (6) 101029/R000658.
- Illman, W.A., 2006. Strong field evidence of directional permeability scale effect in fractured rock. *J. Hydrol.* 319, 227–236.
- Jazayeri Noushabadi, M.R., Jourde, H., Massonnat, G., 2011. Influence of the observation scale on permeability estimation at local and regional scales through well tests in a fractured and karstic aquifer (Lez aquifer, Southern France). *J. Hydrol.* 403, 321–336. <http://dx.doi.org/10.1016/j.jhydrol.2011.04.013>.
- Ji, S.H., Koh, Y.K., 2015. Nonlinear groundwater flow during a slug test in fractured rock. *J. Hydrol.* 520, 30–36.
- Ji, S.H., Lee, H.-B., Yeo, I.W., Lee, K.-K., 2008. Effect of nonlinear flow on DNAPL migration in a rough-walled fracture. *Water Resour. Res.* 44, W11431. <http://dx.doi.org/10.1029/2007WR006712>.
- Krásný Jirí and John M. Sharp, 2003. *Groundwater in Fractured Rocks: IAH Selected Paper Series, volume 9 (IAH - Selected Papers on Hydrogeology)* (First ed).
- Keller, C.E., Cherry, J.A., Parker, B.L., 2014. New method for continuous transmissivity profiling in fractured rock. *Ground Water* 52 (3), 352–367.
- Kurylyk, B.L., Hayashi, M., 2017. Inferring hydraulic properties of alpine aquifers from the propagation of diurnal snowmelt signals. *Water Resour. Res.* 53, 4271–4285. <http://dx.doi.org/10.1002/2016WR019651>.
- Mohnke, O., Yaramanci, U., 2008. Pore size distributions and hydraulic conductivities of rocks derived from magnetic resonance sounding relaxation data using multi-exponential decay time inversion. *J. Appl. Geophys.* 66 (3), 73–81.
- Molz, F.J., Morin, R.H., Hess, A.E., Melville, J.G., Güven, O., 1989. The impeller meter for measuring aquifer permeability variations: evaluation and comparison with other tests. *Water Resour. Res.* 25 (7), 1677–1683.
- National Resources Conservation Service Crow Creek SNOTEL site 2015 United States Department of Agriculture SNOTEL surveys, Available online at <http://wcc.sc.gov.usda.gov/nwcc/site?sitenum=1045>.
- Neuman, S.P., Di Federico, V., 2003. Multifaceted nature of hydrogeologic scaling and its interpretation. *Rev. Geophys.* 41 3/1014.
- Novakowski, K.S., 2000. Fate and transport in fractured rock. In: Lehr, J.H. (Ed.), *Standard Handbook of Environment. Science and Technology*. McGraw Hill 4.74–4.86 Chapter 4.
- Paillet, F.L., 1998. Flow modelling and permeability estimations using borehole flow logs in heterogeneous fractured formations. *Water Resour. Res.* 34 (5), 997–1010.
- Paradis, D., Lefebvre, R., Morin, R.H., Gloaguen, E., 2011. Permeability profiles in granular aquifers using flowmeters in direct-push wells. *Ground Water* 49 (4), 534–547.
- Pepin, N., et al. [Mountain Research Initiative EDW Working Group], 2015. Elevation-dependent warming in mountain regions of the world. *Nat. Clim. Change* 5, 424–430. doi: 10.1038/nclimate2563.
- Quinn, P.M., Cherry, J.A., Parker, B.L., 2011a. Quantification of non-Darcian flow observed during hydraulic testing in fractured sedimentary rock. *Water Resour. Res.* 47 (9), W09533. <http://dx.doi.org/10.1029/2010WR009681>.
- Quinn, P.M., Parker, B.L., Cherry, J.A., 2011b. Using constant head step tests to determine hydraulic apertures in fractured rock. *J. Contam. Hydrol.* 126 (1–2), 85–99.
- Quinn, P.M., Cherry, J.A., Parker, B.L., 2012. Hydraulic testing using a versatile straddle packer system for improved transmissivity estimation in fractured rock boreholes. *Hydrogeol. J.* 20 (8), 1529–1547.
- Quinn, P.M., Parker, B.L., Cherry, J.A., 2013. Validation of non-Darcian flow effects in slug tests conducted in fractured rock boreholes. *J. Hydrol.* 486, 505–518.
- Quinn, P., Cherry, J.A., Parker, B.L., 2015. Combined use of straddle packer testing and FLUTE profiling for hydraulic testing in fractured rock boreholes. *J. Hydrol.* 524, 439–454. <http://dx.doi.org/10.1016/j.jhydrol.2015.03.008>.
- Ranjith, P.G., Darlington, W., 2007. Nonlinear single-phase flow in real rock joints. *Water Resour. Res.* 43, W09502. <http://dx.doi.org/10.1029/2006WR005457>.
- Romm, E.S., 1966. *Flow Characteristics of Fractured Rocks* (in Russian). Nedra, Moscow.
- Rovey, C.W., Niemann, W.L., 2001. Wellskins and slug tests: where's the bias? *J. Hydrol.* 243, 120–132.
- Shapiro, A.M., Hsieh, P.A., 1998. How good are estimates of transmissivity from slug tests in fractured rock? *Ground Water* 36, 37–48. <http://dx.doi.org/10.1111/j.1745-6584.1998.tb01063.x>.
- Snow, D.T., 1965. *A parallel plate model of fractured permeable media*. PhD thesis, University of California Berkeley, Berkeley, CA.
- Tague, C., Grant, G.E., 2009. Groundwater dynamics mediate low-flow response to global warming in snow-dominated alpine regions. *Water Resour. Res.* 45 (7), W07421.
- Zemansky, G.M., McElwee, C.D., 2005. High-resolution slug testing. *Ground Water* 43, 222–230. <http://dx.doi.org/10.1111/j.1745-6584.2005.0008.x>.
- Zimmerman, R.W., Al-Yaarubi, A., Pain, C.C., Grattoni, C.A., 2004. Non-linear regimes of fluid flow in rock fractures. *Int. J. Rock Mech. Min. Sci.* 41, 384.
- Zlotnik, V.A., McGuire, V.L., 1998. Multi-level slug tests in highly permeable formations:

1. Modification of the Springer-Gelhar (SG) model. *Journal of Hydrology* 204, 271–282.
- Zlotnik, V.A., Zurbuchen, B.R., Ptak, T., 2001. The steady-state dipole-flow test for characterization of hydraulic conductivity statistics in a highly permeable aquifer: Horkheimer Insel site, Germany. *Ground Water* 39 (4), 504–516.
- Zlotnik, V.A., Zurbuchen, B.R., 2003. Field study of hydraulic conductivity in a heterogeneous aquifer: comparison of single-borehole measurements using different instruments. *Water Resour. Res.* 39 (4), 1101. <http://dx.doi.org/10.1029/2002WR001415>.